Article

Developmental Cell

Epidermal hydrodynamics controls water homeostasis of shoot meristems for plant adaptation to terrestrial environments

Graphical abstract

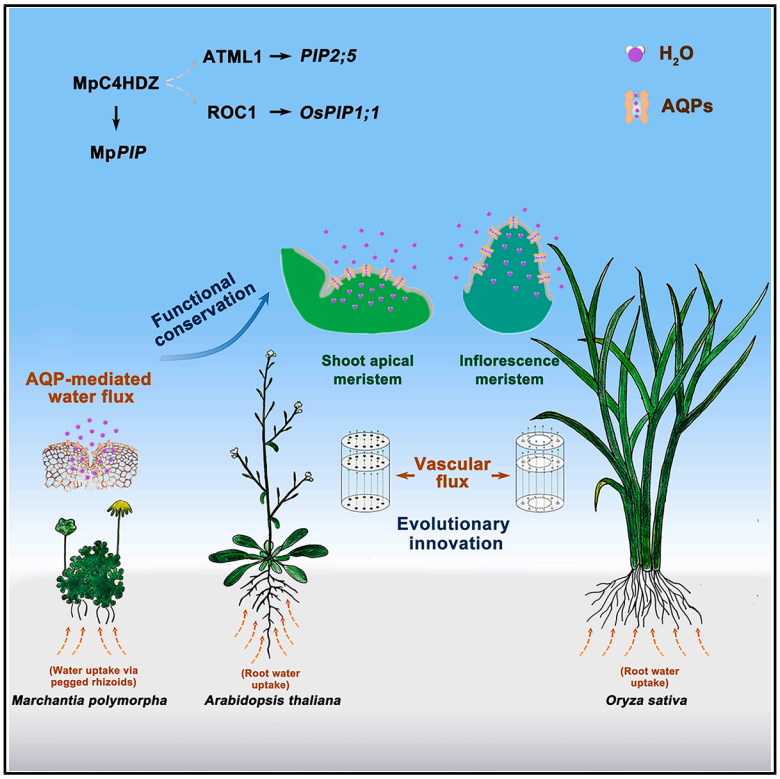

Authors

Yimin Zhu, Xianmiao Zhu, Simin Bi, ..., Ertao Wang, Minbiao Ji, Weibing Yang

Correspondence

wbyang@cemps.ac.cn

In brief

Zhu et al. uncover an evolutionarily conserved water transport pathway in the epidermis of plant shoot meristems that maintains water homeostasis and regulates stem cell activity. This epidermal hydrodynamic system is shaped by climate-driven selection, contributing to plant adaptation to terrestrial environments.

Highlights

- Plant shoot meristem is preserved within a humidified microenvironment
- An epidermal hydraulic pathway regulates water homeostasis of the shoot meristem
- Hydraulic exchange via the shoot meristem epidermis is conserved during plant evolution
- Epidermal hydrodynamics is subject to climate-driven selection in natural populations

Zhu et al., 2026, Developmental Cell *61*, 1–14
January 14, 2026
https://doi.org/10.1016/j.devcel.2025.09.007

CellPress

Please cite this article in press as: Zhu et al., Epidermal hydrodynamics controls water homeostasis of shoot meristems for plant adaptation to terrestrial environments, Developmental Cell (2025), https://doi.org/10.1016/j.devcel.2025.09.007

Developmental Cell

CellPress
OPEN ACCESS

Article

Epidermal hydrodynamics controls water homeostasis of shoot meristems for plant adaptation to terrestrial environments

Yimin Zhu,[1,2] Xianmiao Zhu,[1,2,11] Simin Bi,[3,11] Dan Teng,[4,11] Muhammad Tahir,[5,11] Yangxuan Liu,[1,11] Long Wang,[1] Huanhuan Liu,[6] Tingting Wen,[1] Leyao Zhu,[1,8] Zhenquan Li,[1,2] Xing Chen,[1,2] Minhua Zhang,[1] Wenjuan Cai,[1,9] Zhijun Liu,[1] Mingyue Zheng,[4] Yu Zhang,[7] Ji-Ming Gong,[1] Jia-Wei Wang,[1] Zuhua He,[1] Lihong Li,[5] Ertao Wang,[1] Minbiao Ji,[3] and Weibing Yang[1,10,12,*]

[1]Key Laboratory of Plant Carbon Capture, CAS Centre for Excellence in Molecular Plant Sciences (CEMPS), Institute of Plant Physiology and Ecology, Chinese Academy of Sciences (CAS), Shanghai 200032, China
[2]University of Chinese Academy of Sciences, Beijing, China
[3]Department of Physics, State Key Laboratory of Surface Physics, Shanghai Key Laboratory of Metasurfaces for Light Manipulation, Endoscopy Center and Endoscopy Research Institute, Zhongshan Hospital, Fudan University, Shanghai 200433, China
[4]State Key Laboratory of Drug Research, Shanghai Institute of Materia Medica, CAS, Shanghai 201203, China
[5]School of Materials Science and Engineering, University of Science and Technology Beijing, 30 Xueyuan Road, Beijing 100083, China
[6]Key Laboratory of Bio-resource and Eco-environment of Ministry of Education, College of Life Sciences, Sichuan University, Chengdu 610065, China
[7]Key Laboratory of Synthetic Biology, CEMPS, CAS, Shanghai 200032, China
[8]Key Laboratory of Plant Stress Biology, State Key Laboratory of Cotton Biology, School of Life Sciences, Henan University, Kaifeng 475004, China
[9]Core Facility Center, CEMPS, CAS, Shanghai 200032, China
[10]CAS-JIC Center of Excellence for Plant and Microbial Sciences (CEPAMS), Beijing, China
[11]These authors contributed equally
[12]Lead contact
*Correspondence: wbyang@cemps.ac.cn
https://doi.org/10.1016/j.devcel.2025.09.007

SUMMARY

Water uptake and redistribution represent a significant challenge for plant colonization of land. While vascular plants have evolved specialized structures for water transport, how water homeostasis is maintained in meristematic tissues remains elusive. Here, we show that the *Arabidopsis* shoot meristem develops within a high-humidity niche. The homeodomain leucine zipper (HD-ZIP) transcription factor ARABIDOPSIS THALIANA MERISTEM LAYER 1 (ATML1) and its regulatory target *PIP2;5* establish a water conduit across L1 cells to facilitate hydraulic exchange with the surrounding microenvironment. The ATML1-PIP2;5 module regulates stem cell activity in response to humidity fluctuations and is associated with local adaptation to arid climates in natural populations. Transcriptional activation of water flux by class IV homeodomain-leucine zipper (C4HDZ) proteins predates the emergence of vascular systems, contributing to hydraulic response in the liverwort *Marchantia polymorpha*. Our results reveal an evolutionarily conserved epidermal hydraulic pathway that integrates developmental patterning with environmental sensing, highlighting a fundamental role for the shoot meristem in shaping plant adaptation in terrestrial habitats.

INTRODUCTION

Crop seed production and nutritional security are threatened by the rising prevalence of floods and drought associated with climate change.[1,2] Water, as one of the most limiting factors for plant growth, facilitates the movement of dissolved minerals, nutrients, hormones, and other signaling molecules. Additionally, water flux into the cells generates hydrostatic turgor pressure, which, coupled with cell wall elasticity, promotes plant cell expansion, organ emergence, and hygroscopic movements.[3–6] The interplay between water transport and perception plays pivotal roles in orchestrating plant developmental plasticity.[7–15]

Water also serves as a driving force of plant evolution.[16] When plants conquered land 470 million years ago (mya), one of the most significant challenges was desiccation.[17,18] To cope with water deprivation in the terrestrial environments, developmental adaptations such as surface cuticles and stomata have been innovated that allow for the prevalence of tissue hydration and exchange of CO_2, respectively.[19–23] Additionally, a specialized

Please cite this article in press as: Zhu et al., Epidermal hydrodynamics controls water homeostasis of shoot meristems for plant adaptation to terrestrial environments, Developmental Cell (2025), https://doi.org/10.1016/j.devcel.2025.09.007

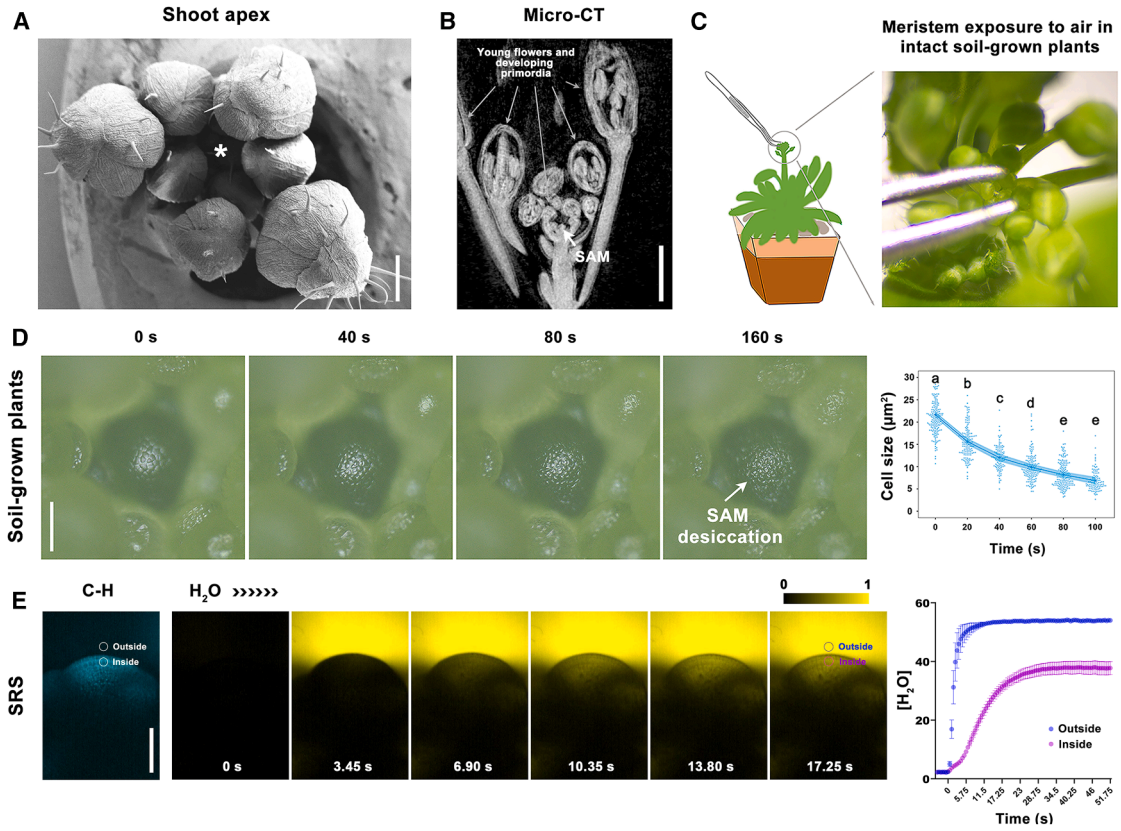

Figure 1. A humidity niche maintains water homeostasis of shoot meristem in *Arabidopsis thaliana*

(A) A cryo-scanning electron microscopy (SEM) image of a wild-type (WT) *Arabidopsis* shoot apex. The star indicates the location of the SAM. Scale bar, 50 μm.

(B) The interior structure of the shoot apex revealed by micro-CT scanning. Scale bar, 1 mm.

(C) Experimental setup for shoot meristem exposure to the air in intact plants grown in soil.

(D) Morphology of non-dissected SAMs upon air exposure (60% RH). Data shown in the right panel represent changes in cell size during meristem dehydration. The regression line represents the cell size with the 95% confidence interval (CI) shaded. Letters indicate statistically significant differences, as calculated by one-way ANOVA with Tukey's multiple comparisons test ($p < 0.05$). Scale bar, 50 μm.

(E) Direct observation of liquid water movement in the SAMs ($n = 6$) by SRS microscopy, demonstrating rapid water influx. The right panel shows the time course changes in H_2O concentrations (calculated based on the intensities of the Raman signals) across the selected regions of interest (ROIs) outside and inside of the SAM, as indicated by two circles in the left panel. Data represent means ± SEM. Time constant = 9.0 ± 0.5 s for "inside." Scale bar, 50 μm. Please see Methods S1 for further details of the SRS assay.

See also Figure S1.

internal hydraulic conduit system, the vasculature, was developed for long-distance transport of water.[24,25] At the cellular level, hydraulic conductivity is largely influenced by aquaporins, a family of water channels that mediate intercellular water movement across the plasma membranes.[26,27] The activity of aquaporin is tightly regulated through transcription, tissue- or cell-specific expression,[28,29] and phosphorylation modifications.[30–32]

Another key innovation of land plants is the shoot apical meristem (SAM), which harbors stem cells that undergo active division and differentiation, giving rise to all above-ground tissues.[33,34] Stem cell activity within the shoot meristem not only contributes to three-dimensional (3D) growth, enabling the establishment of erect plant architecture,[35,36] but also determines inflorescence size in flowering plants, thus impacting grain yield in cereal crops.[37] Despite its crucial roles in plant growth and reproductive success, it remains unclear how the shoot meristem survives desiccation pressure under humidity fluctuations in terrestrial environments.

Here, we discover that plant shoot meristems reside within a humidified microenvironment. This local humidity is perceived by an ATML1-PIP2;5 transcriptional module on the epidermis. The epidermal conduit fine-tunes water homeostasis of the shoot meristem and influences stem cell division activity under fluctuating environmental humidity. Our study unveils a molecular framework governing water transport and stem cell maintenance in plant shoot meristems, highlighting the crucial roles of epidermal hydraulics in guiding plant adaptation to local climates.

RESULTS

The shoot meristem responds rapidly to moisture changes

The SAM of plants exists in unique microhabitats, where developing primordia and young flowers physically enclose stem cell reservoirs within a chamber-like structure (Figures 1A and 1B). Removing the flowers and exposing the *Arabidopsis*

SAMs to ambient air triggered stem cell shrinkage within 2 min (Figures S1A and S1B; Video S1), indicating rapid water loss and subsequent reduction in turgor pressure. By contrast, maintaining SAMs in enclosed Petri dishes completely prevented desiccation (Figures S1C–S1E). These results suggest that floral or leaf organs surrounding the shoot meristem may impede airflow and thus create a humidified microenvironment at the shoot apex for moisture maintenance. To test this hypothesis, we reduced local moisture by gently repositioning the flowers to fully expose the SAMs in soil-grown plants (Figure 1C). Disruption of the humidity niche led to shoot meristem desiccation within 2 min (Figure 1D; Video S1), similar to that observed in the dissected SAMs, suggesting that the shoot meristem undergoes active water evaporation when exposed to ambient air.

To monitor hydrodynamics in the shoot meristem non-invasively, we leveraged stimulated Raman scattering (SRS) microscopy, a label-free imaging technique developed in biomedical research for the detection of specific metabolites.[38] With SRS microscopy, the distinct vibrational signal of O-H and O-D stretches enable the detection of H_2O and D_2O molecules at 3,270 and 2,500 cm^{-1}, respectively. The SAMs were incubated with D_2O in a microfluidic chamber, and the SRS microscopy was tuned to target H_2O (Methods S1). When the D_2O was replaced with H_2O, we observed an increase of SRS signals of H_2O in the SAM, which reached saturation at around 30 s (Figure 1E), indicating that liquid water can be absorbed by the shoot meristem. Therefore, the humidified air may prevent evaporation and, in the meantime, provide an additional water source for moisture maintenance of the shoot stem cells.

Systematic gene expression reveals PIP2;5 as an epidermal aquaporin in *A. thaliana*

In the absence of stomata, rapid water loss from the shoot meristem upon air exposure may occur via alternative mechanisms, potentially involving vapor diffusion from the apoplastic space and aquaporin-mediated transmembrane water movement (Figures 2A and 2B).[39] To investigate the hydrodynamics of aquaporin-mediated water transport at the SAM, we generated fluorescence reporters for the 12 plasma membrane intrinsic proteins (*PIPs*) and 5 tonoplast intrinsic proteins (*TIPs*) with detectable expression in our RNA sequencing (RNA-seq) data.[40] Confocal microscopy analysis detected fluorescence signals for 5 *PIP* genes in the SAM cells (including *PIP1;3*, *PIP1;5*, *PIP2;5*, *PIP2;6*, and *PIP2;7*), whereas all the *TIPs* examined were expressed in the underlying stem regions (Figure S2A).

The majority of SAM-expressed *PIPs* showed enrichment in the inner layers (Figure 2C), except for *PIP2;5*, which exhibited high and specific expression in the epidermal (L1) cells (Figures 2D and S2C). The L1 layer expression pattern of the *PIP2;5* promoter reporter was consistent with its mRNA distribution as examined by mRNA *in situ* hybridization (Figure S2B). PIP2;5 proteins were localized to the plasma membrane (Figures 2E and S2D) and displayed overlapping expression with the auxin efflux carrier PIN-FORMED1 (PIN1) (Figure S2E). In mature tissues such as leaves and stems, the expression levels of *PIP2;5* were much lower (Figure S2F), suggesting a predominant activity of PIP2;5 in the L1 cells of the shoot meristem.

ATML1 activates *PIP2;5* expression in L1 cells of the *Arabidopsis* shoot meristem

In silico analysis of the *PIP2;5* promoter sequence revealed two putative L1-box motifs (CATTTA/TAAATG) (Figure 2F), which are recognized by ATML1, a class IV homeodomain-leucine zipper (C4HDZ) transcription factor.[41–44] Electrophoretic mobility shift assay (EMSA) and yeast-one-hybrid assay reveal that ATML1 could directly bind to *PIP2;5* promoter (Figures 2G and 2H). To establish ATML1 as a regulator of *PIP2;5* transcription in *Arabidopsis*, we generated a *pATML1::GFP-ATML1* translational reporter (Figure 2I). Chromatin immunoprecipitation (ChIP) of ATML1-bound DNA in *pATML1::GFP-ATML1* shoot apex with an anti-GFP antibody revealed enrichment of *PIP2;5* promoter fragments (Figure 2J). In a dual-luciferase reporter assay, the expression of the *pPIP2;5::LUC* reporter was markedly enhanced when co-expressed with ATML1 (Figure 2K).

Activation of *PIP2;5* expression by ATML1 was further verified by the observation that mutations in *ATML1* and its closest homolog, *PROTODERMAL FACTOR 2* (*PDF2*),[45] led to dramatically reduced *PIP2;5* expression in the *atml1-1 pdf2-1* double mutant (Figures S2G–S2I). Moreover, mutation of the L1-box motifs of the *PIP2;5* promoter (Figure S2J) diminished its transcriptional activity (Figures S2K and S2L). Collectively, these findings indicate the existence of an ATML1-PIP2;5 transcriptional module that presumably regulates epidermal hydraulics at the shoot apex.

PIP2;5 contributes to water homeostasis of the *Arabidopsis* shoot meristem

PIP2;5 is a functional water channel that was able to promote water transport in the protoplast swelling assay (Figure S3A). To assess its functions in plants, we isolated a homozygous T-DNA insertion mutant for *PIP2;5*. SRS imaging showed that water uptake in the SAMs of the *pip2;5* mutant was partially inhibited (Figure S3B), suggesting reduced hydraulic conductivity. In agreement with this, when the shoot meristems of *pip2;5* plants were exposed to air, the average dehydration time was measured at 203 ± 53 s, which was 1.6-fold longer than that of the wild-type SAMs (127 ± 44 s) (Figures 3A and 3B), indicating a delayed response to a reduction in air humidity.

We further investigated the influence of increased air humidity on SAM growth. Wild-type and *pip2;5* plants were grown at 40% relative humidity (RH) until the bolting stage, after which they were shifted to 90% RH for 7 days. Analysis of SAM morphologies revealed a decrease in SAM size in response to increased air humidity (Figures 3C and 3D). The smaller SAMs under high humidity were not likely caused by compromised cell growth, as the size of L1 cells was only slightly reduced from 24.5 ± 6.5 μm^2 at 40% RH to 23.9 ± 6.4 μm^2 at 90% RH. Instead, the number of L1 cells under 90% RH was reduced to less than half of that under 40% RH (Figures 3E and 3F). The decrease in cell division activity upon high-humidity treatment was further confirmed by a time course live imaging assay (Figure S3E).

Reduced shoot meristem growth upon exposure to high humidity still occurred in *pip2;5*, but to a lesser extent, leading to more cells and larger SAMs in *pip2;5* plants compared with the wild type under 90% RH (Figures 3C–3F). These phenotypes were also verified in an additional *PIP2;5* mutant allele generated through CRISPR-Cas9 genome editing (Figures S3B, S3F, and

Please cite this article in press as: Zhu et al., Epidermal hydrodynamics controls water homeostasis of shoot meristems for plant adaptation to terrestrial environments, Developmental Cell (2025), https://doi.org/10.1016/j.devcel.2025.09.007

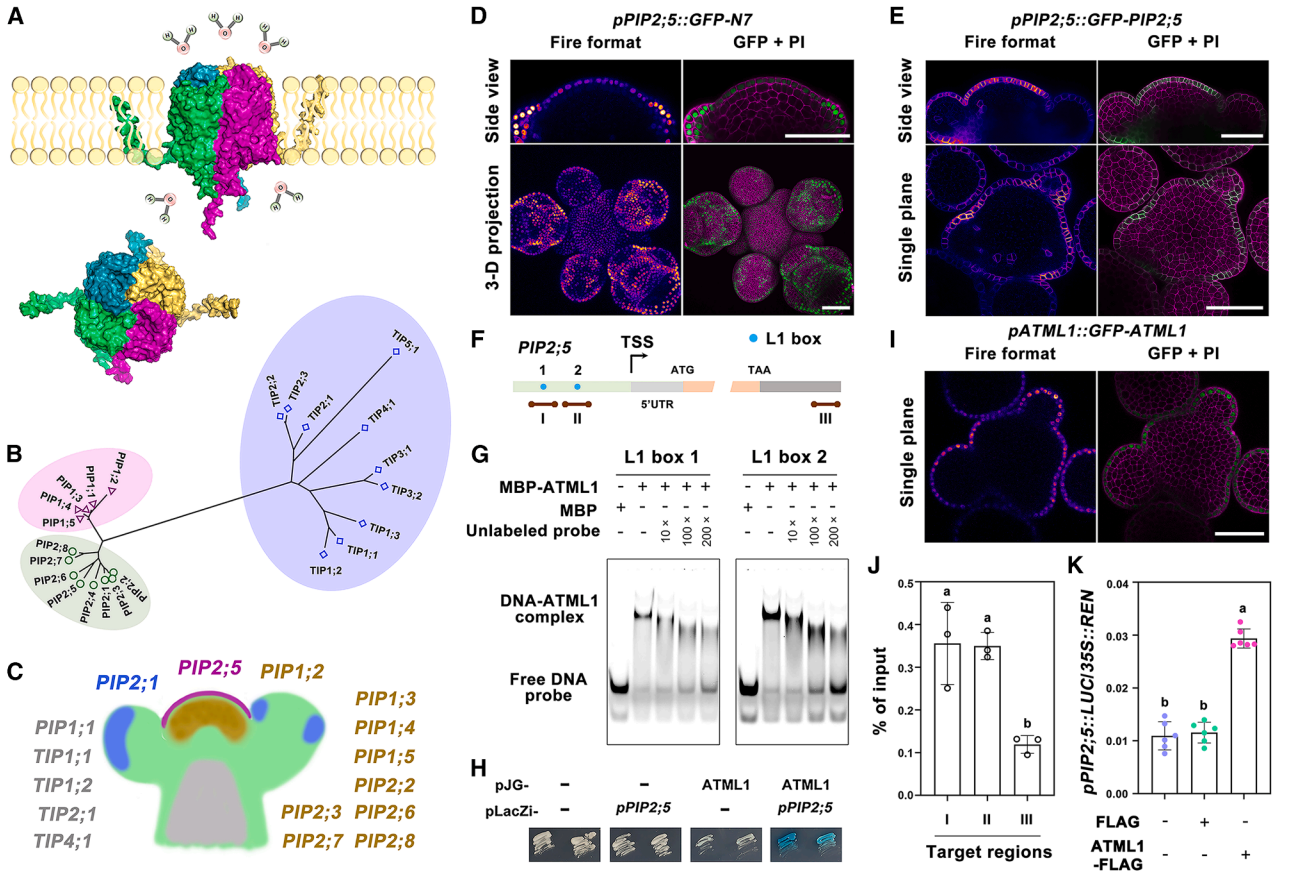

Figure 2. The ATML1-PIP2;5 module establishes a water conduit across the L1 cells of the *Arabidopsis* shoot meristem

(A) Schematic representation of aquaporin-mediated water transport. The tetramer structure was computed using AlphaFold based on the amino acid sequence of PIP1;2 and illustrated by the PyMol Molecular Graphics System (version 2.0; Schrödinger).

(B) A phylogenetic tree of aquaporins in *Arabidopsis*.

(C) Summary of the expression patterns of the transcriptional reporters of aquaporin genes at the SAM.

(D and E) Enriched expression of *PIP2;5* transcriptional (D) and translational (E) reporters in the L1 cells. GFP signals are shown with the Fire look-up table. The cell walls are stained with propidium iodide (PI) and shown in magenta. Scale bars, 50 μm.

(F) Distribution of L1 box motifs within the promoter region of *PIP2;5*.

(G) EMSA demonstrating the binding of ATML1 to Cy5-labeled DNA probes containing *PIP2;5* promoter fragments.

(H) Interaction of ATML1 with the *PIP2;5* promoter, as detected by the yeast-one-hybrid assay.

(I) Expression pattern of ATML1 in the L1 cells. Scale bar, 50 μm.

(J) ChIP-qPCR analysis to assess the binding of ATML1 to the *PIP2;5* promoter. The abundance of each fragment of the *PIP2;5* promoter was determined by qPCR.

(K) Dual-luciferase assay demonstrating the transcriptional activation of *PIP2;5* by ATML1. Firefly luciferase (LUC) and Renilla luciferase (REN) were expressed under the control of the *PIP2;5* promoter and *35S* promoter, respectively. Shown are the ratios of LUC to REN activity. Data are from six biological replicates. Data (J) and (K) represent means ± SD. Letters indicate statistically significant differences, as calculated by one-way ANOVA with Tukey's multiple comparisons test ($p < 0.05$).

See also Figure S2.

S3G). Together, the SRS microscopy, SAM desiccation, and humidity shift assays revealed lower sensitivity of the SAMs of the *pip2;5* mutants in response to changes in air humidity, suggesting that epidermis-expressed *PIP2;5* plays a role in the maintenance of water homeostasis and cell division activity in the shoot meristem.

ATML1-PIP2;5 module regulates molecular responses to air humidity in *A. thaliana*

Under 40% RH, the *pip2;5* mutant exhibited reduced plant size and smaller SAMs, which could be fully rescued by the GFP-PIP2;5 fusion protein (Figures S3C and S3D), suggesting a beneficial role of PIP2;5-mediated epidermal water flux in promoting shoot meristem development and plant growth. To verify the functional significance of PIP2;5 in the L1 cells, we used the *ATML1* promoter to drive *GFP-PIP2;5* expression in the *pip2;5* mutant background. The epidermis-specific expression of *GFP-PIP2;5* mRNA and its cognate proteins in the *pip2;5; pATML1::GFP-PIP2;5* plants was confirmed by RNA fluorescence *in situ* hybridization (FISH) and confocal microscopy, respectively (Figures 3G and 3H). Phenotypic analysis and humidity shift assays demonstrate that expression of *PIP2;5* only

Please cite this article in press as: Zhu et al., Epidermal hydrodynamics controls water homeostasis of shoot meristems for plant adaptation to terrestrial environments, Developmental Cell (2025), https://doi.org/10.1016/j.devcel.2025.09.007

CellPress
OPEN ACCESS

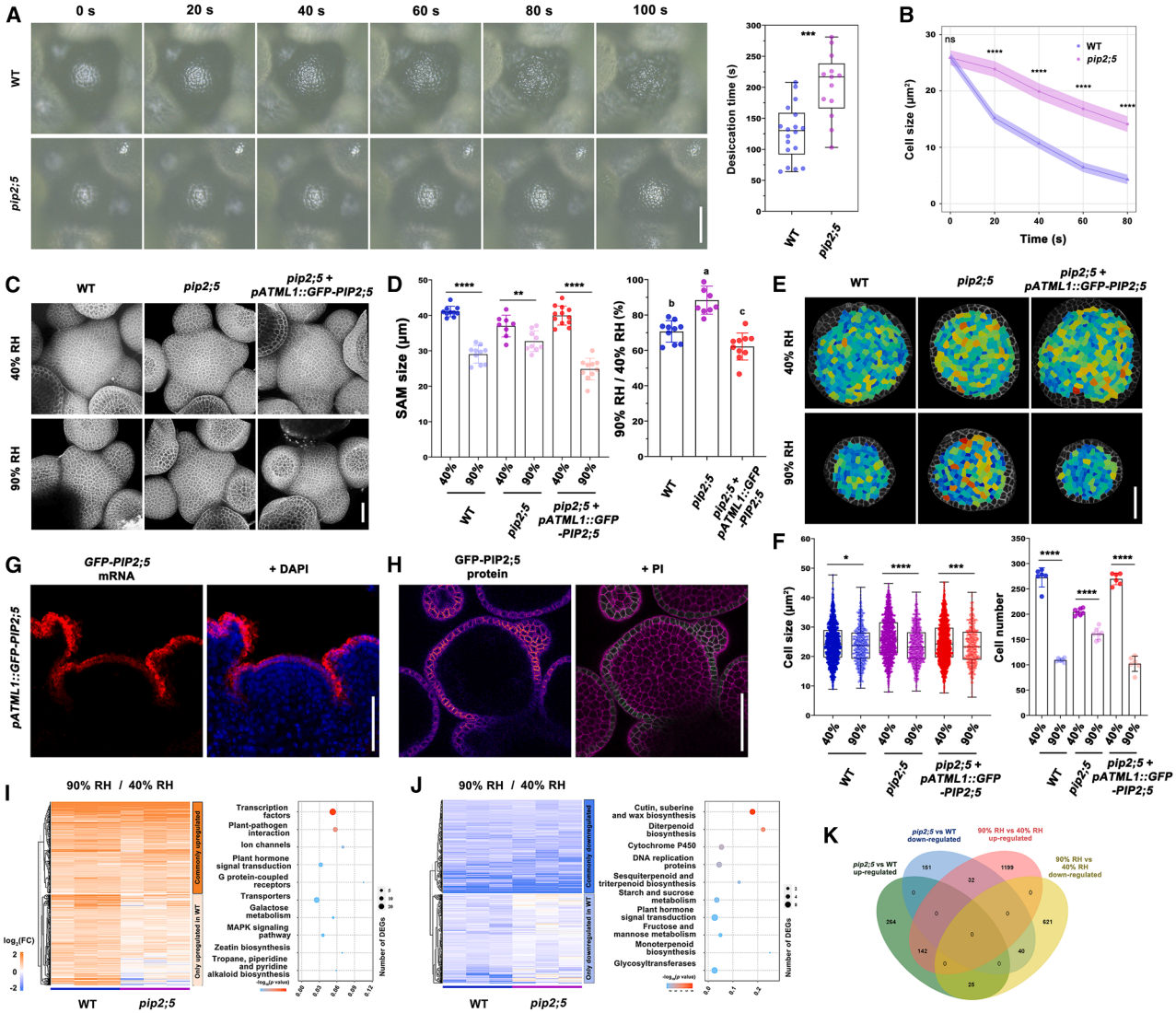

Figure 3. Epidermal PIP2;5 regulates hydraulic homeostasis in *Arabidopsis* shoot meristem

(A) Comparison of the desiccation process of WT (Col-0) (n = 18) and *pip2;5* (n = 13) shoot meristems after exposure to the air (24°C, RH 60%). The desiccation time was estimated as the interval between the start of SAM exposure to the air until no further cell cremation occurred. Boxplots indicate the median (box center line), 25%, 75% (box), and the whiskers extend to the minima and maxima. Scale bars, 50 μm.

(B) Quantification of the cell size of WT (n = 6 SAMs) and *pip2;5* (n = 6 SAMs) shoot meristems at different time points after exposure to the air. The regression line represents the cell size with the 95% CI shaded.

(C) Comparison of WT, *pip2;5*, and *pip2;5;pATML1::GFP-PIP2;5* SAM morphologies under different air humidity levels. The cell walls are stained with PI and shown in gray. Scale bar, 30 μm.

(D) Quantification of SAM size of WT (40% RH, n = 10; 90% RH, n = 10), *pip2;5* (40% RH, n = 8; 90% RH, n = 9), and *pip2;5;pATML1::GFP-PIP2;5* (40% RH, n = 12; 90% RH, n = 10) plants under 40% RH and 90% RH. SAM size is estimated by measuring the radius of 3D projections of the confocal stacks. The ratio of SAM size is calculated by normalizing the sizes of individual SAMs under 90% RH to the average size of the SAMs under 40% RH. Data represent means ± SD.

(E) The effect of air humidity on the size of WT, *pip2;5*, and *pip2;5;pATML1::GFP-PIP2;5* SAM cells. The segmented L1 (epidermal) cells are displayed as heatmaps showing relative cell area. Scale bar, 30 μm.

(F) Quantification of the size and number of L1 cells in WT (40% RH, n = 6; 90% RH, n = 6), *pip2;5* (40% RH, n = 7; 90% RH, n = 7), and *pip2;5;pATML1::GFP-PIP2;5* (40% RH, n = 6; 90% RH, n = 6) SAMs following different humidity treatments, demonstrating a suppression of cell division activity under high humidity. Data represent means ± SD.

(G) Detection of *PIP2;5* expression in *pip2;5;pATML1::GFP-PIP2;5* shoot meristems using mRNA FISH with a *GFP* RNA probe. Scale bar, 20 μm.

(H) Examination of GFP-PIP2;5 fluorescence signals in the shoot meristems of *pip2;5;pATML1::GFP-PIP2;5*, showing specific expression in the L1 cells. Scale bars, 50 μm.

(I and J) Hierarchical clustering and functional annotation of genes upregulated (I) and downregulated (J) by high humidity, based on their relative expression levels determined by RNA-seq in the shoot apices of WT and *pip2;5* plants. FC, fold change.

(legend continued on next page)

Please cite this article in press as: Zhu et al., Epidermal hydrodynamics controls water homeostasis of shoot meristems for plant adaptation to terrestrial environments, Developmental Cell (2025), https://doi.org/10.1016/j.devcel.2025.09.007

in the L1 cells fully restored the growth (Figure S3H) and water response phenotypes of the *pip2;5* mutant (Figures 3C–3F). Thus, we postulate that the ATML1-PIP2;5 module constitutes a layer of highly efficient water channels, which mediates hydraulic exchange between the shoot meristem and the local high-humidity microenvironment.

To determine whether the distinct response of *pip2;5* SAMs to high humidity was a specific effect of humidity or an indirect consequence of altered growth, we performed transcriptome analysis. Wild-type and *pip2;5* plants were grown under 40% RH until the bolting stage, after which they were shifted to high humidity (90% RH) and grown for an additional 24 h. The shoot apices were dissected for RNA-seq analysis. In wild-type shoot apices, high humidity enhanced the expression of genes associated with hypoxia, abscisic acid (ABA), and ethylene responses (Figure 3I), whereas the genes involved in cuticular wax biosynthesis were downregulated (Figure 3J), indicating conserved transcriptomic adjustments to water excess in the shoot meristems.[46] We also found that high humidity suppressed the expression of genes regulating DNA replication and sugar metabolism (Figure 3J), in line with the decreased cell proliferation activity under this condition (Figure S3E).

High-humidity-induced transcriptome reprogramming was greatly abolished in the *pip2;5* mutant, with 49.7% (683/1,373) of the upregulated genes and 48.8% (335/686 genes) of the downregulated genes in wild-type plants showing no significant change in *pip2;5* shoot apex upon high-humidity treatment. Moreover, 38.7% (167/431) of the upregulated and 32.3% (72/223) of the downregulated genes in *pip2;5* compared with wild type at 40% RH were also affected by 90% RH treatment (Figure 3K), suggesting a role of *PIP2;5* in molecular response to air humidity. In further support of this, both transcript and protein levels of PIP2;5 were reduced under 90% RH compared with 40% RH, coinciding with decreased expression of ATML1 (Figures S3I–S3N). These data collectively suggest that *PIP2;5*, driven by ATML1 in the L1 cells of the shoot meristem, was involved in the control of transcriptional and cellular responses to humidity fluctuations.

Differential water transport activities of PIP2;5 natural variants

Arabidopsis plants are geographically distributed under different air humidity regimes,[47,48] displaying a wide range of root hydraulic profiles.[49] We investigated whether *PIP2;5* was involved in plant adaptation to local humidity. By comparing the genomic sequences of *PIP2;5* from 1,135 *Arabidopsis* accessions,[50] we identified 16 single-nucleotide polymorphisms (SNPs) within the *PIP2;5* coding region, with only three being non-synonymous nucleotide polymorphisms (Figure S4A; Table S1). Based on these three SNPs, the *Arabidopsis* accessions can be grouped into seven haplotypes, Hap0 to Hap6. Hap0 and Hap6 account for 76.6% and 19.5%, respectively, of all the accessions analyzed, thus representing the dominate haplotypes of *PIP2;5* in natural populations (Figure 4A).

Among the three amino acid changes between Hap0 and Hap6 (Figure 4B), Ile55 is specific to PIP2;5, and all the other PIPs contain Val at this site. In addition, Asn70/Ser70 and Thr75/Ala75 are situated in the extended extracellular loop A consensus of PIP2 family members (except for PIP2;7 and PIP2;8) (Figures S4B and S4C). Molecular dynamics simulations, using the open conformation of the SoPIP2;1 structure as a template, indicate that substitutions with Ser70 and Ala75 in Hap6 led to closure of loop A and rearrangement of the transmembrane helices toward the interior space of the channel (Figures 4C and 4D; Methods S2). To assess the functional relevance of *PIP2;5* natural variants, we compared the water transport activities of Hap0 and Hap6 in *Xenopus* oocyte cells. Both Hap0 and Hap6 proteins were localized to the membrane (Figure 4E). Osmotic permeation assays showed that Hap0 exhibited a water permeability (P_f) value of $(3.8 \pm 0.6) \times 10^{-2}$ cm/s, which was reduced to $(2.7 \pm 0.5) \times 10^{-2}$ cm/s for Hap6 (Figure 4F). The diminished water transport activity of Hap6 is consistent with molecular dynamics simulations, where a high probability of a discontinuous water file was observed in the Hap6 channel.

To verify the functional differences between Hap0 and Hap6 in *Arabidopsis* plants, we expressed *GFP-PIP2;5-Hap0* and *GFP-PIP2;5-Hap6* in the *pip2;5* mutant under the control of the *PIP2;5* promoter. With SRS microscopy, we show that the reduced water import activity of the *pip2;5* SAMs could be rescued by *GFP-PIP2;5-Hap0* but only partially by *GFP-PIP2;5-Hap6* (Figure S4D). In addition, the *pip2;5;pPIP2;5::GFP-PIP2;5-Hap0* plants exhibited a reduction in SAM size similarly to that of wild-type plants under high-humidity treatment, whereas this effect was less pronounced for the *pip2;5;pPIP2;5::GFP-PIP2;5-Hap6* plants (Figures 4G and 4H). Together, these results suggest a weaker activity of PIP2;5-Hap6 as compared with PIP2;5-Hap0.

Natural *PIP2;5* variation in *Arabidopsis* accessions is associated with dry habitats

To further validate the association of Hap0 and Hap6 haplotypes with shoot meristem humidity response, we examined the effect of humidity on meristem growth in natural accessions. Among the 24 *Arabidopsis* accessions we tested (12 for Hap0 and 12 for Hap6), 13 did not bolt even after prolonged growth under long-day conditions. The remaining 11 accessions that could bolt include six Hap0 and five Hap6, which were subjected to a humidity shift assay. We found that, compared with the accessions with Hap0, the Hap6 plants generally produced smaller SAMs and exhibited a reduced response to high humidity (Figures 4I–4L), consistent with the decreased water transport activity of PIP2;5-Hap6.

Due to the genetic variation between natural *Arabidopsis* accessions, additional loci may mask the effects of *PIP2;5* haplotypes on humidity response. Therefore, we analyzed a population of near-isogenic lines (NILs) generated from two local accessions, Tibet and Sichuan, which contain Hap0 and Hap6,

(K) Venn diagram showing that the high-humidity-responsive genes were already dysregulated in *pip2;5* SAMs under low-humidity conditions.
Letters (D) indicate statistically significant differences, as calculated by one-way ANOVA with Tukey's multiple comparisons test ($p < 0.05$). *$p < 0.05$, **$p < 0.01$, ***$p < 0.001$, and ****$p < 0.0001$ (two-tailed *t* test) (A, B, D, and F).
See also Figure S3.

Developmental Cell
Article

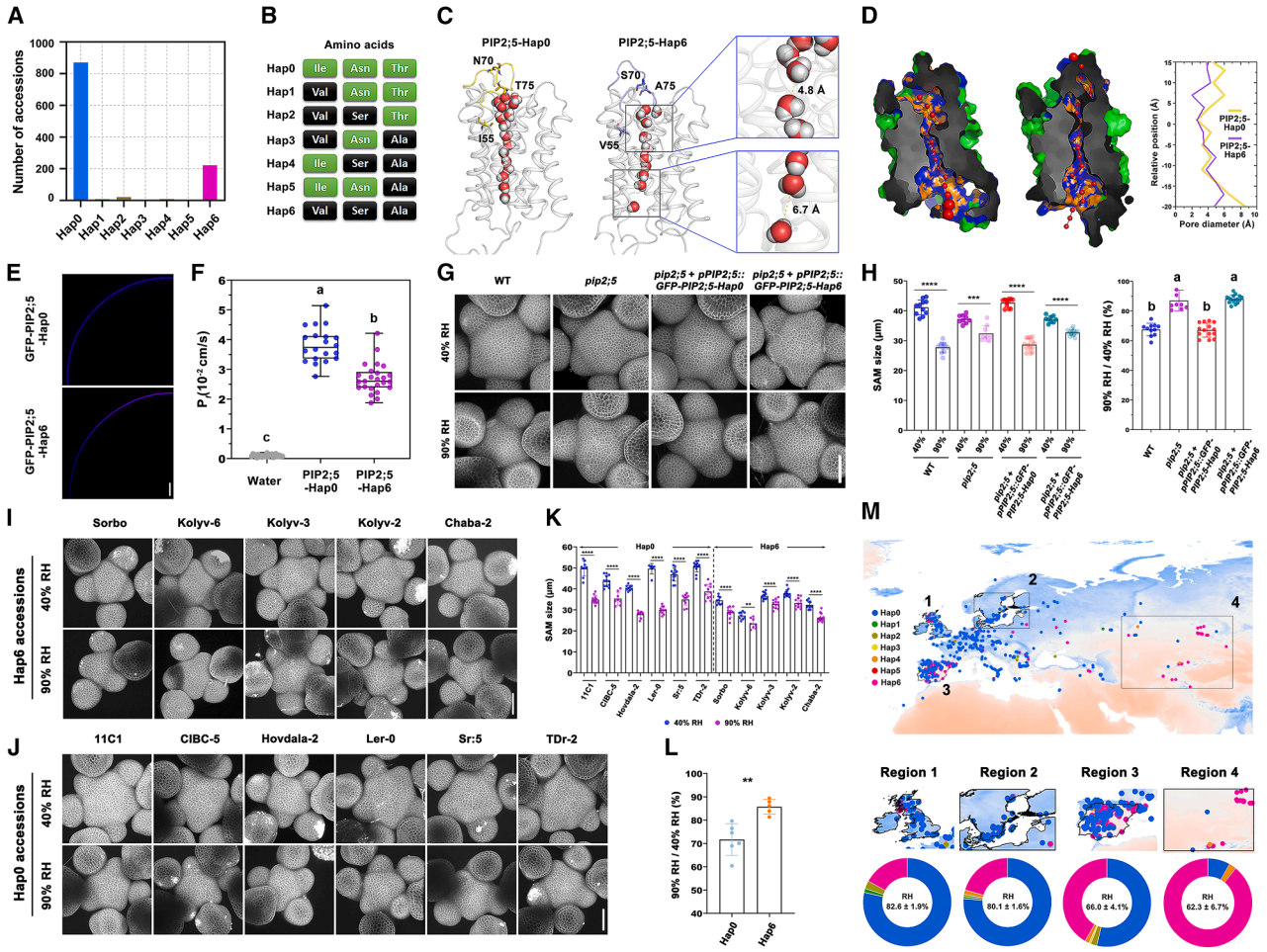

Figure 4. Natural variation of *PIP2;5* allele in *Arabidopsis* accessions associates with arid climates

(A) Frequency distribution of the *PIP2;5* haplotypes in *Arabidopsis* accessions.

(B) Amino acid variations of PIP2;5 haplotypes at the positions of Ile55 (I55), Asn70 (N70), and Thr75 (T75).

(C and D) Molecular dynamics simulation of PIP2;5 Hap0 and Hap6 proteins, showing the open conformations of Hap0 and Hap6 (C) and the pore diameter (D). 3D structure was simulated using the open conformation of SoPIP1 (PDB: 2B5F) as a template. A continuous and single-file configuration of water molecules was observed in Hap0, whereas in Hap6 the distance between successive water molecules was increased, resulting in a discontinuous water file.

(E) Subcellular localization of PIP2;5 Hap0 and Hap6 in *Xenopus* oocyte cells. Scale bar, 100 μm.

(F) Osmotic water permeability of *Xenopus* oocytes expressing PIP2;5 Hap0 ($n = 20$) and Hap6 ($n = 25$). Water serves as a control ($n = 25$).

(G) Comparison of the SAM morphologies of WT, *pip2;5*, *pip2;5;pPIP2;5::GFP-PIP2;5-Hap0*, and *pip2;5;pPIP2;5::GFP-PIP2;5-Hap6* plants under different air humidity levels. Scale bar, 50 μm.

(H) Quantification of SAM size of WT (40% RH, $n = 11$; 90% RH, $n = 11$), *pip2;5* (40% RH, $n = 9$; 90% RH, $n = 9$), *pip2;5;pPIP2;5::GFP-PIP2;5-Hap0* (40% RH, $n = 12$; 90% RH, $n = 14$), and *pip2;5;pPIP2;5::GFP-PIP2;5-Hap6* (40% RH, $n = 9$; 90% RH, $n = 16$) plants under 40% RH and 90% RH.

(I and J) Morphologies of the SAMs under different air humidity levels in *Arabidopsis thaliana* accessions with Hap6 (I) and Hap0 (J). Scale bars, 50 μm.

(K and L) Quantification of the shoot meristem size of *Arabidopsis* accessions harboring Hap0 or Hap6 under different air humidity levels. High-humidity-suppressed SAM growth is less pronounced in accessions with the Hap6 haplotype.

(M) Geographical distribution of *PIP2;5* haplotypes, demonstrating an increase in the frequency of PIP2;5 Hap6 with decreasing local air humidity. The pie chart (bottom) illustrates the haplotype frequencies in each region. The RH distribution map depicts an average of monthly surface air RH from January 1979 to December 2022 (Climate Data Store).

Boxplots (F) indicate the median (box center line), 25%, 75% (box), and the whiskers extend to the minima and maxima. Data (H), (K), and (L) represent means ± SD. Letters (F) and (H) indicate statistically significant differences, as calculated by one-way ANOVA with Tukey's multiple comparisons test ($p < 0.05$). $^{**}p < 0.01$, $^{***}p < 0.001$, and $^{****}p < 0.0001$ (two-tailed *t* test) (H, K, and L).

See also Figure S4.

respectively.[51] In these NILs, the Tibet (Hap0) genomic fragments were replaced by those from the Sichuan (Hap6) accession. Using a set of simple sequence repeat (SSR) markers with polymorphisms between Sichuan and Tibet accessions, we characterized one NIL, designated as NIL$^{PIP2;5\text{-}Sic}$, which contains the *PIP2;5* locus of Sichuan with minimal introgression of additional genomic fragments (Figures S4E and S4F). A humidity shift assay demonstrates that NIL$^{PIP2;5\text{-}Sic}$ (Hap6) SAMs

Please cite this article in press as: Zhu et al., Epidermal hydrodynamics controls water homeostasis of shoot meristems for plant adaptation to terrestrial environments, Developmental Cell (2025), https://doi.org/10.1016/j.devcel.2025.09.007

exhibited a reduced response to high humidity compared with the Tibet accession (Hap0) (Figures S4G–S4I). However, our whole-genome re-sequencing revealed that NIL$^{PIP2;5\text{-}Sic}$ also contains additional Sichuan fragments on chromosomes 1, 2, and 4, which may potentially influence humidity response. Nevertheless, the NIL data, combined with the results from the natural accessions and the Hap0/6 complementation lines, support the conclusion that natural variations in *PIP2;5* are related to plant humidity response in *Arabidopsis*.

We further explored the geographic distribution of *PIP2;5* haplotypes, which revealed an association of *PIP2;5* haplotypes with air humidity (Pearson's χ^2 test, $p < 0.0001$). *Arabidopsis* accessions harboring Hap0 were found to be dominant in higher air humidity regions, including central Europe, whereas Hap6 was enriched in areas with generally low air humidity, such as Spain (Figure 4M). Reduced water transport activity of Hap6 may facilitate cellular water conservation, thereby contributing to growth fitness in dry habitats. The correlation between *PIP2;5* variants and local air humidity in natural populations suggests that hydraulic conductivity at the shoot meristem may have undergone climate-driven natural selection.

HD-ZIP activation of epidermal water flux is conserved in monocot rice

Considering the essential role of water transport in plant adaptation to terrestrial environments, we next explored the conservation of the SAM epidermal hydraulics. Orthologs of ATML1 and PIPs were detected in land plants, but they are absent in the single-cell alga *Chlamydomonas reinhardtii* (Figure 5A; Table S2). Rice (*Oryza sativa*), a monocot crop that diverged from *Arabidopsis* ~150 mya ago,[52] was selected for further comparative analysis. The rice shoot meristems are enclosed by developing young leaves and leaf sheaths (Figure S5A), which undergo rapid dehydration upon exposure to the air (Figure S5B). Among the 11 rice *PIPs*, *OsPIP1;1*, *OsPIP2;1*, and *OsPIP2;6* were highly expressed in the inflorescence meristem[53] (Figure 5B), with *OsPIP1;1* exhibiting enriched expression in the L1 cells (Figure 5C), overlapping with the expression domains of the rice ATML1 ortholog RICE OUTERMOST CELL-SPECIFIC 1 (ROC1).[54] In the *OsPIP1;1* promoter, we identified two L1 motifs, both of which could be recognized by ROC1 (Figure 5D). Moreover, the promoter activity of *OsPIP1;1* was enhanced in the presence of ROC1 (Figure 5E). These results demonstrate that ROC1 binds to *OsPIP1;1* promoter and activates its expression in the epidermal cells of rice shoot meristem.

To investigate the functions of *OsPIP1;1* in rice, we focused on an *ospip1;1* mutant generated by CRISPR-Cas9.[55] We found that, compared with the wild-type Zhonghua 11 (ZH11), the dehydration of the shoot meristems was much slower in *ospip1;1* (Figure 5F), suggesting that *OsPIP1;1* contributes to the hydraulic balance of rice shoot meristems. Phenotypical analysis showed that both the length of the panicles and the number of primary and secondary branches were reduced in *ospip1;1* (Figure 5G). As the rice panicle develops from the inflorescence meristem, the smaller panicles in *ospip1;1* may imply decreased meristem activity.

A systematic comparison of the genomic sequences of *OsPIP1;1* across 3,025 rice accessions identified multiple SNPs within the 3,000 bp promoter region and two SNPs in its coding region (SNP-27044566 and SNP-27044764) (Table S1). As these two coding variants were found in only a small proportion of the accessions (1.66% and 3.11%, respectively), we focused our analysis on a promoter variant (SNP-27044056) located within the second L1-box motif of the *OsPIP1;1* promoter (Figure S5C). Based on this SNP, the rice cultivars can be grouped into two haplotypes: SNP^T and SNP^C (Figure S5D). Analysis of the geographic distribution revealed that SNP^T is more prevalent in high-humidity regions, whereas SNP^C exhibits a broad distribution with slight enrichment in low-humidity areas (Pearson's χ^2 test, $p < 0.0001$) (Figure S5E). Using an EMSA, we found that the SNP^C promoter had reduced affinity to the transcription factor ROC1 (Figure S5F). Although ROC1 could still induce the activity of the SNP^C promoter, it was much weaker than that of the SNP^T promoter (Figure S5G). In agreement with this, the expression levels of *OsPIP1;1* in the shoot meristems of accessions harboring SNP^C were generally lower than those harboring SNP^T (Figure S5H). Based on these data, we propose that the epidermal water conduit is conserved in rice and that natural variation in the *OsPIP1;1* promoter influences ROC1 binding affinity, leading to altered gene expression and likely differential hydraulic conductivity in the rice shoot meristem.

Epidermal moisture extraction is traced back to *M. polymorpha*

To further track the evolutionary history of this epidermis hydraulic system, we focused on *M. polymorpha*, a liverwort that diverged from vascular plants at the dawn of land plant evolution.[56,57] The thallus (shoot) meristem of *M. polymorpha* is covered by ventrally produced scales that curl around the apical notch. In addition, within this region are numerous mucilage cells.[58] Thus, the apical meristem of *M. polymorpha* is protected in an analogous manner to the shoot meristem in *Arabidopsis*, within a high-humidity microenvironment. Compared with angiosperms, the aquaporin gene family in *M. polymorpha* was greatly expanded, with 14 genes belonging to the *PIP* family (Figure S6A). However, among them, only *Mp2g13930* and *Mp4g17210* showed detectable expression in tissue-specific RNA-seq analysis (Figure S6B).[56] These two genes were designated as Mp*PIP1* and Mp*PIP2*, respectively, according to their phylogenetic relationship with the *Arabidopsis* orthologs. When expressed in *Xenopus* oocytes, both MpPIP1 and MpPIP2 showed water transport activity (Figures S6C and S6D).

We generated *pro*Mp*PIP1:*Mp*PIP1-Citrine* and *pro*Mp*PIP2:* Mp*PIP2-Citrine* reporter lines and found that both genes were expressed in the epidermal cells of vegetative thalli with high enrichment at the meristematic notch (Figures 6A and 6B). In the promoters of Mp*PIP1* and *MpPIP2*, we identified two and one putative L1 box motifs, respectively, which could be bound by MpC4HDZ (Mp7g09710), the ortholog of *Arabidopsis* ATML1 (Figure 6C). A dual-luciferase assay demonstrated that MpC4HDZ enhanced the promoter activity of Mp*PIP1* and *MpPIP2* (Figure 6D). To further verify the control of Mp*PIP1* and *MpPIP2* expression by MpC4HDZ in *M. polymorpha*, we generated an Mp*c4hdz-1* mutant using a dual guide RNA (gRNA) CRISPR-Cas9

Please cite this article in press as: Zhu et al., Epidermal hydrodynamics controls water homeostasis of shoot meristems for plant adaptation to terrestrial environments, Developmental Cell (2025), https://doi.org/10.1016/j.devcel.2025.09.007

CellPress
OPEN ACCESS

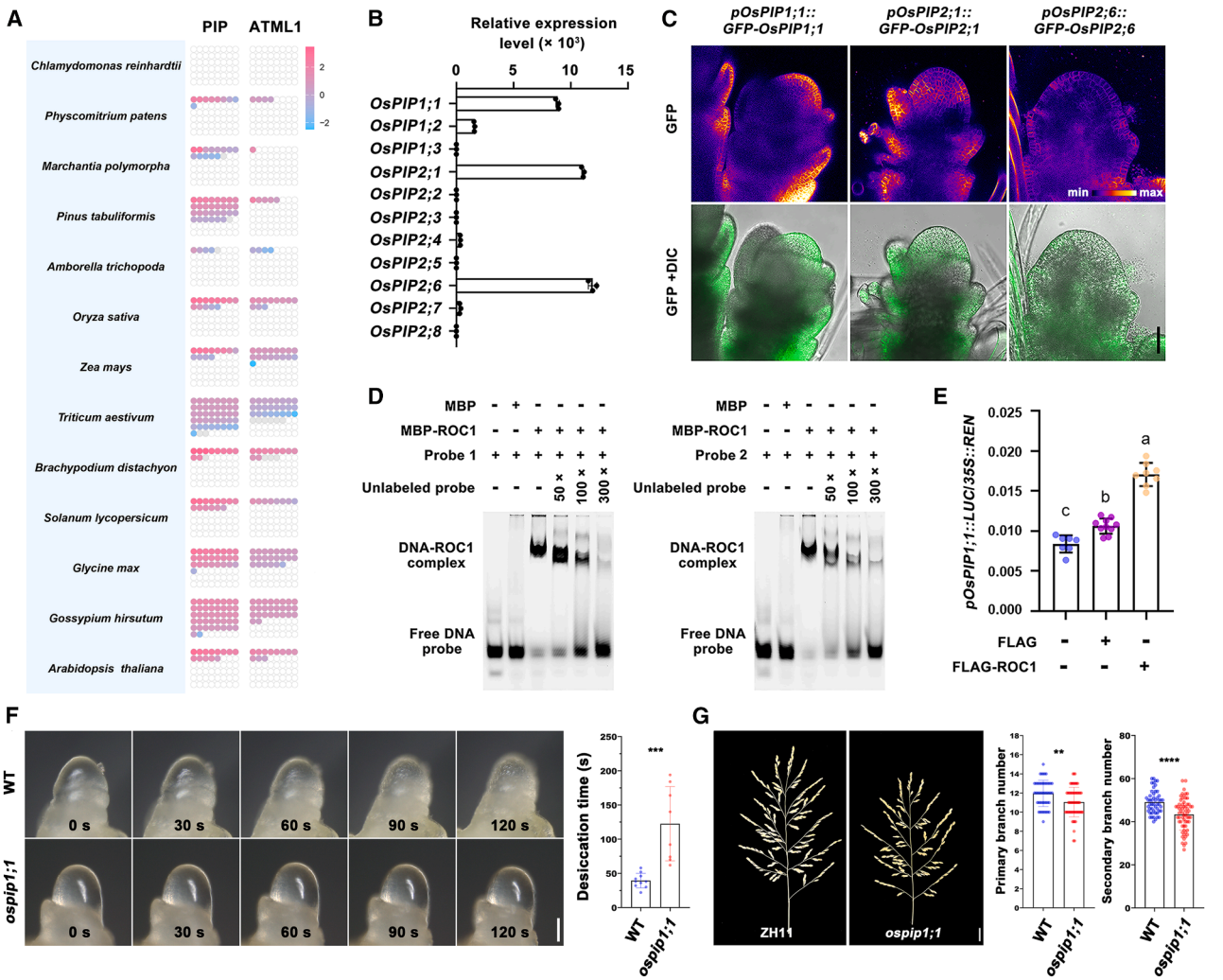

Figure 5. Activation of *OsPIP1;1* expression by ROC1 in the epidermis of rice inflorescence meristem

(A) Analysis of *PIP* and *C4HDZ* orthologs in 13 representative green lineage plant species. Filled circles indicate the presence of orthologs, while open circles represent the absence. Different colors of the filled circles represent heatmaps, which are constructed based on the average expression levels (log_{10}) of each gene in various tissues. The orthologous genes with no detectable expression are labeled in gray.

(B) Expression levels of rice aquaporin genes in the inflorescence meristem. Shown are transcripts per million (TPM) values detected by RNA-seq.

(C) Expression patterns of translational reporters of OsPIP1;1, OsPIP2;1, and OsPIP2;6 in the floret meristem. Scale bar, 50 μm.

(D) EMSA demonstrating the binding of ROC1, the rice ortholog of ATML1, to the promoter regions of *OsPIP1;1*.

(E) Activation of *OsPIP1;1* transcription by ROC1. Firefly LUC and REN were expressed under the control of the *OsPIP1;1* promoter and *35S* promoter, respectively. Shown are the ratios of LUC to REN activity.

(F) Representative images showing the desiccation process of WT (ZH11) ($n = 10$) and *ospip1;1* ($n = 8$) shoot meristems after exposure to the air (24°C, RH 60%). Scale bar, 50 μm.

(G) Effect of *OsPIP1;1* mutation on rice panicle development. The numbers of primary and secondary branches of the panicles are shown in the right (ZH11, $n = 50$; *ospip1;1*, $n = 63$). Scale bar, 2 cm.

Data (B) and (E)–(G) represent means ± SD. Letters (E) indicate statistically significant differences, as calculated by one-way ANOVA with Tukey's multiple comparisons test ($p < 0.05$). $^{**}p < 0.01$, $^{***}p < 0.001$, and $^{****}p < 0.0001$ (two-tailed *t* test) (F and G).

See also Figure S5.

system.[59] Mp*c4hdz-1* harbors a deletion in the putative disorder domain, representing a weak allele. Compared with the wild-type (Tak-1) plants, the expression levels of Mp*PIP1* and *MpPIP2* were greatly reduced in Mp*c4hdz-1* (Figure 6E), indicating that MpC4HDZ was a positive regulator of Mp*PIP1* and *MpPIP2* expression. Accordingly, the activation of aquaporin gene expression by the HD-ZIP class of transcription factors appears to be an early evolutionary innovation of land plants.

The MpC4HDZ-PIP module contributes to water response and erect growth in *M. polymorpha*

M. polymorpha has neither vasculature nor internal water-conducting cells.[60] While the pegged rhizoids have been implicated

Please cite this article in press as: Zhu et al., Epidermal hydrodynamics controls water homeostasis of shoot meristems for plant adaptation to terrestrial environments, Developmental Cell (2025), https://doi.org/10.1016/j.devcel.2025.09.007

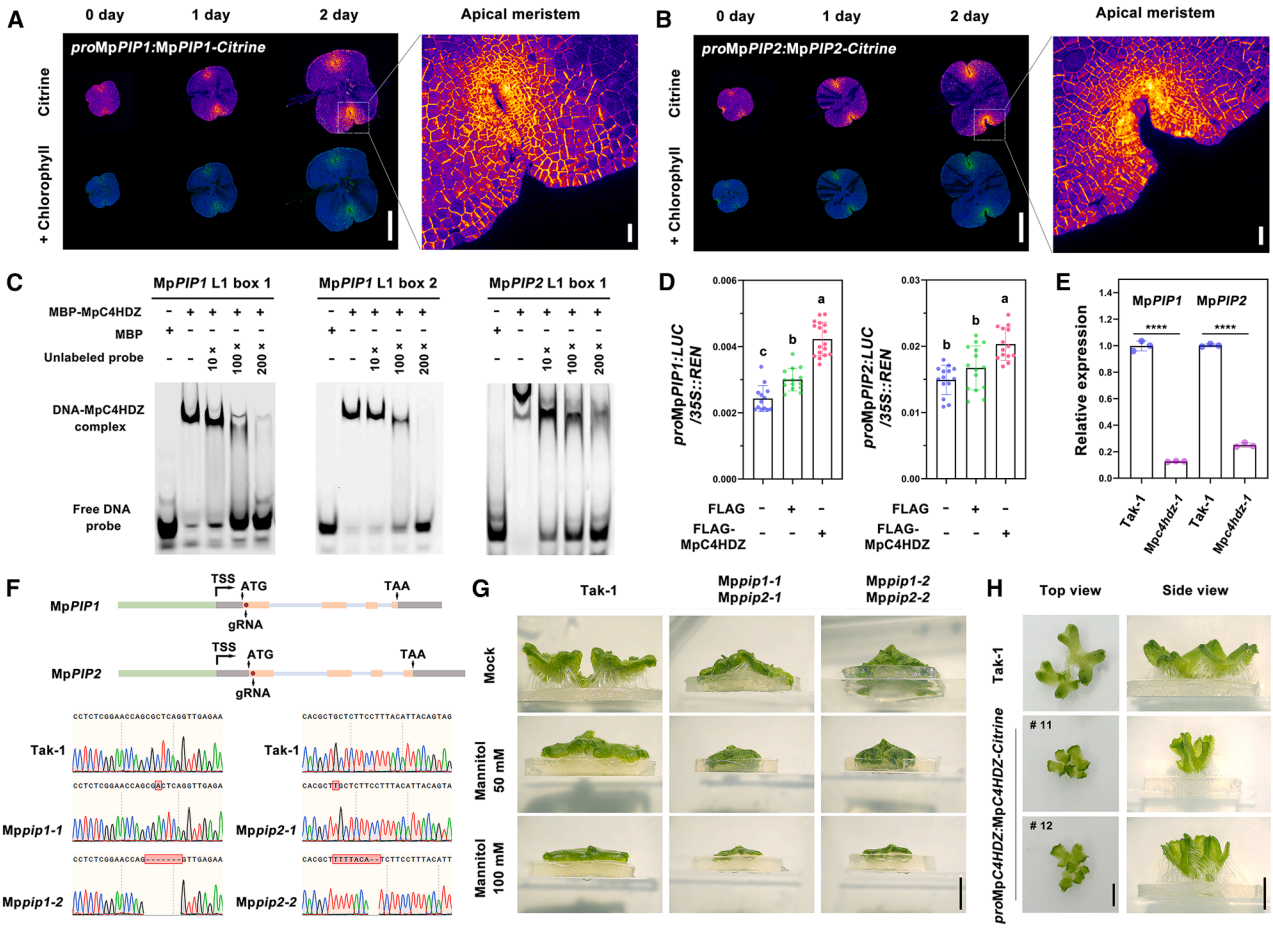

Figure 6. The MpC4HDZ-Mp*AQP* module regulates water response and upward growth in *M. polymorpha*

(A and B) Expression patterns of *M. polymorpha* aquaporins Mp*PIP1* and Mp*PIP2* under the control of their native promoters. The outline of the thalli was delineated by the autofluorescence signals of the chlorophyll (shown in blue). Scale bars, 200 μm (left panel) and 20 μm (right panel).

(C) EMSA demonstrating the binding of MpC4HDZ, the ortholog of ATML1 in *M. polymorpha*, to the promoter regions of Mp*PIP1* and Mp*PIP2*.

(D) Transcriptional activation of Mp*PIP1* and Mp*PIP2* by MpC4HDZ.

(E) Comparison of Mp*PIP1* and Mp*PIP2* expression in Tak-1 and Mp*c4hdz-1* mutants.

(F) Generation of Mp*PIP1* and Mp*PIP2* null mutants by CRISPR-Cas9.

(G) Morphological analysis of Tak-1 (WT), Mp*pip1-1* Mp*pip2-1*, and Mp*pip1-2* Mp*pip2-2* plants grown on Gamborg B5 medium supplemented with various concentrations of mannitol. Shown are side views of the thalli. Scale bars, 0.5 cm.

(H) Mp*C4HDZ* overexpression promoted erect growth of the thalli. Scale bars, 0.5 mm.

Data (D) and (E) represent means ± SD. Letters (D) indicate statistically significant differences, as calculated by one-way ANOVA with Tukey's multiple comparisons test ($p < 0.05$). ****$p < 0.0001$ (two-tailed *t* test) (E).

See also Figure S6.

in water absorption through capillarity,[61–63] the role of aquaporin-mediated intercellular water transport has not been investigated in *M. polymorpha*. To elucidate the functions of MpPIP1 and MpPIP2, we generated two independent double mutants, Mp*pip1-1* Mp*pip2-1* and Mp*pip1-2* Mp*pip2-2* (Figure 6F). Compared with the upward tropic growth of Tak-1, the Mp*pip1-1* Mp*pip2-1* and Mp*pip1-2* Mp*pip2-2* mutant thalli were closely appressed to the surface of and frequently penetrated into the medium (Video S2). These phenotypes resembled those of wild-type plants cultured on medium supplemented with mannitol (Figure 6G). Conversely, in Mp*C4HDZ* overexpression plants (Figure S6E), the thalli showed enhanced upright growth (Figure 6H), giving rise to an erect habit.

To investigate the functions of Mp*PIP1* and *MpPIP2* in water response, we performed a humidity shift assay. Tak-1 and the Mp*pip1* Mp*pip2* mutant plants were grown on soil with constant covering and regular watering, which creates a high-humidity condition that resembles the natural habitats of *M. polymorpha*. When the lid was open to reduce the air humidity with minimal impact on soil moisture, both Mp*pip1-1* Mp*pip2-1* and Mp*pip1-2* Mp*pip2-2* mutant plants became severely dehydrated after 24 h, whereas the Tak-1 thalli remained moist albeit suppressed growth (Figure S6F). These results indicate that mutation of Mp*PIP1* and *MpPIP2* compromised moisture absorption and/or maintenance of the thalli, suggesting that C4HDZ transcription factor-activated expression of MpPIP1 and MpPIP2 proteins in the

Please cite this article in press as: Zhu et al., Epidermal hydrodynamics controls water homeostasis of shoot meristems for plant adaptation to terrestrial environments, Developmental Cell (2025), https://doi.org/10.1016/j.devcel.2025.09.007

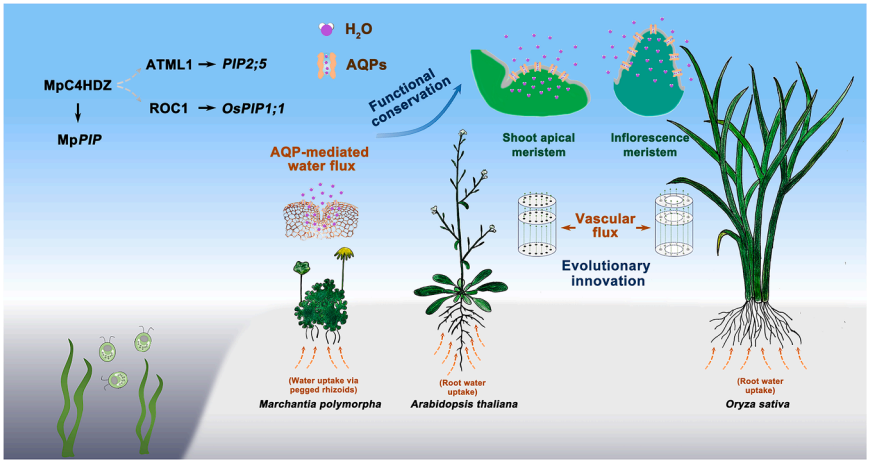

Figure 7. A schematic illustration of the epidermal hydrodynamics across plant lineages

Schematic illustration of epidermal hydrodynamics across plant lineages. Water uptake, transport, and maintenance are crucial for plant survival in terrestrial habitats. The shoot meristems of vascular plants develop within a humidified microenvironment, which reduces evaporation and preserves moisture of the stem cells. The HD-ZIP IV transcription factor-activated expression of aquaporins establishes a water conduit in the epidermis of the shoot meristem, which responds to local moisture changes and fine-tunes stem cell activity. Epidermal hydraulics can be traced back to the liverwort *M. polymorpha*, representing a deeply conserved mechanism for moisture response and plant adaptation to dry environments.
See also Figure S7.

surface cells facilitates water exchange between the thalli and the high-humidity environment, similarly to that conferred by PIP2;5 in *Arabidopsis*.

Hydrodynamics in the shoot meristems of tomato, soybean, and maize

In addition to *Arabidopsis*, rice, and *M. polymorpha*, we further investigated the hydraulic exchange in the shoot meristems of tomato (*Solanum lycopersicum*), soybean (*Glycine max*), and maize (*Zea mays*) (Figure S7A). Micro-computed tomography (micro-CT) scanning reveals that in these species, the shoot meristems are also closely surrounded by developing young organs and undergo rapid dehydration upon exposure to air (Figures S7B–S7D). Through SRS microscopy, we show that external liquid water can be absorbed by the shoot meristems of these plants at varying flux rates (Figures S7E and S7F), likely reflecting the differences in the cellular organization of shoot meristems among these species. These results suggest that hydraulic exchange between the shoot meristem and its microenvironment might be a conserved phenomenon across different plant clades.

DISCUSSION

The apical location exposes the shoot meristem to the risk of desiccation due to its distance from soil water sources. We show that, in various plant species, the shoot meristem is preserved within a humidity microenvironment. An evolutionarily conserved transcriptional module, activated by the HD-ZIP transcription factors and acting through the water channel aquaporins, perceives this local moisture within the shoot meristem microenvironment and modulates stem cell proliferation in response to fluctuations in ambient humidity levels. Our finding suggests that, in addition to the root, the shoot meristem also senses and responds to water availability (Figure 7).

Given the crucial roles of ambient humidity in plant development, it is not surprising that the epidermal hydraulics would have been subject to climate-driven selection. This hypothesis was supported by the identification of *PIP2;5-Hap6*, a natural allele prevalent in dry habitats that shows reduced water channel activity. The geographic distribution and physiological activity of PIP2;5-Hap6 suggest that it may represent a drought-survival allele, and its frequency in the natural population will likely increase under the selection pressure exerted by extreme drought events in future climates.[64] As high water use efficiency is a major target of crop breeding,[65] our characterization of epidermal hydrodynamics at the growing apex, along with its evolutionary conservation, may provide new strategies for the breeding of climate-resilient crops.

Limitations of the study

We show that the epidermal water conduit mediates shoot meristem response to fluctuations in environmental humidity. While SRS microscopy allows for the tracking of liquid water movement into the shoot meristem, it remains unclear whether the vapor phase of water in humidified air can be directly absorbed by the stem cells. Another limitation of this study is that, although we have shown that the water conductivity in the epidermis is suppressed by high humidity, further studies will help to understand how the ATML1-PIP2;5 module responds to moisture changes.

RESOURCE AVAILABILITY

Lead contact

Further information and requests for resources and reagents should be directed to and will be fulfilled by the lead contact, Weibing Yang (wbyang@cemps.ac.cn).

Materials availability

Constructs and reagents in this study will be made available upon request, but a completed materials transfer agreement may be required if there is potential for commercial application.

Data and code availability

- The raw sequence data generated during this study are available at the NCBI Gene Expression Omnibus (GEO; https://www.ncbi.nlm.nih.gov/geo/) under accession number GEO: GSE256367.
- This paper does not report the original code.
- Any additional information required to reanalyze the data reported in this paper is available from the lead contact upon request. The raw SRS data, gene expression quantification, and fluorescence intensity measurements have been deposited at Mendeley Data and are publicly available at https://doi.org/10.17632/tnjzrbnsm9.1.

ACKNOWLEDGMENTS

We would like to thank John Bowman, Caroline Dean, Henrik Jönsson, and Raymond Wightman for helpful discussions and comments on the manuscript. We are grateful to Elliot Meyerowitz for the support during the early phase of this project, which was conducted at the Sainsbury Laboratory, Cambridge University. We thank Yun Zhou, Benoit Landrein, Xiangyang Yu, Miqi Xu, Dawei Yan, and NASC for materials; Richard Smith for suggestions on MorphoGraphX analysis; Aram Gurzadyan for help with the shoot meristem desiccation assay; and Jianpeng Ao for assistance with SRS microscopy. This work was supported by the CAS Project for Young Scientists in Basic Research (YSBR-108), the CAS Strategic Priority Research Program (type-B; XDB0630200 and XDB27030107), the National Key Research and Development Program of China (2022YFF1001803), and the National Natural Science Foundation of China (NSFC) (32170325).

AUTHOR CONTRIBUTIONS

W.Y. conceived the project. Y. Zhu, X.Z., and W.Y. designed the study, performed the experiments, and analyzed the data. S.B. carried out the SRS microscopy analysis. Y.L. analyzed the RNA-seq data and haplotype distribution. D.T. performed the molecular dynamics simulations analysis. T.W., Z. Liu, and M. Zhang. contributed to the water transport assay in *Xenopus* oocyte cells. L. Z., Z. Li., X.C., and W.C. contributed to reporter gene expression analysis. L.W. contributed to *M. polymorpha* transformation and fluorescence reporter assay. L.L., H.L., M.T., M. Zheng, J.-M.G., Y. Zhang, J.-W.W., Z.H., E.W., and M.J. contributed to new reagents and data analysis. Y. Zhu, X.Z., and W.Y. interpreted the data and wrote the manuscript with contributions from Y.L., D.T., and S.B. All authors discussed and commented on the manuscript.

DECLARATION OF INTERESTS

The authors declare no competing interests.

STAR★METHODS

Detailed methods are provided in the online version of this paper and include the following:

- KEY RESOURCES TABLE
- EXPERIMENTAL MODEL AND STUDY PARTICIPANT DETAILS
  - Plant materials and growth conditions
  - Bacterial strains
- METHOD DETAILS
  - Plasmid construction
  - *Arabidopsis*, rice, and *M. polymorpha* transformation
  - Protein expression and purification
  - Confocal microscopy imaging of *Arabidopsis* shoot meristem
  - Confocal microscopy imaging of rice inflorescence meristem
  - Confocal microscopy imaging of *M. polymorpha*
  - Confocal data analysis
  - Cell size analysis of shoot meristems during desiccation
  - Stimulated Raman scatter (SRS) microscopy
  - Chromatin immunoprecipitation assay
  - Electrophoretic mobility shift assay
  - Transactivation assay
  - mRNA *in situ* hybridization
  - RNA fluorescence *in situ* hybridization (RNA FISH)
  - Yeast one-hybrid assay
  - RNA sequencing analysis
  - Quantitative real-time reverse-transcription PCR (qRT-PCR)
  - Immunoblotting assay
  - Osmotic permeation assay in *Xenopus laevis* oocytes
  - Analysis of transgene copy number
  - Protoplast swelling assay
  - Whole-genome re-sequencing
  - Characterization of PIP and ATML1 orthologues
- QUANTIFICATION AND STATISTICAL ANALYSIS

SUPPLEMENTAL INFORMATION

Supplemental information can be found online at https://doi.org/10.1016/j.devcel.2025.09.007.

Received: April 25, 2024
Revised: November 6, 2024
Accepted: September 5, 2025

REFERENCES

1. Mickelbart, M.V., Hasegawa, P.M., and Bailey-Serres, J. (2015). Genetic mechanisms of abiotic stress tolerance that translate to crop yield stability. Nat. Rev. Genet. *16*, 237–251. https://doi.org/10.1038/nrg3901.
2. Hirt, H., Al-Babili, S., Almeida-Trapp, M., Martin, A., Aranda, M., Bartels, D., Bennett, M., Blilou, I., Boer, D., Boulouis, A., et al. (2023). PlantACT! - how to tackle the climate crisis. Trends Plant Sci. *28*, 537–543. https://doi.org/10.1016/j.tplants.2023.01.005.
3. Cosgrove, D.J. (1993). Water uptake by growing cells: an assessment of the controlling roles of wall relaxation, solute uptake, and hydraulic conductance. Int. J. Plant Sci. *154*, 10–21. https://doi.org/10.1086/297087.
4. Ali, O., Mirabet, V., Godin, C., and Traas, J. (2014). Physical models of plant development. Annu. Rev. Cell Dev. Biol. *30*, 59–78. https://doi.org/10.1146/annurev-cellbio-101512-122410.
5. Dumais, J., and Forterre, Y. (2012). "Vegetable dynamicks": The role of water in plant movements. Annu. Rev. Fluid Mech. *44*, 453–478. https://doi.org/10.1146/annurev-fluid-120710-101200.
6. Coen, E., and Cosgrove, D.J. (2023). The mechanics of plant morphogenesis. Science *379*, eade8055. https://doi.org/10.1126/science.ade8055.
7. Scharwies, J.D., and Dinneny, J.R. (2019). Water transport, perception, and response in plants. J. Plant Res. *132*, 311–324. https://doi.org/10.1007/s10265-019-01089-8.
8. Péret, B., Li, G., Zhao, J., Band, L.R., Voß, U., Postaire, O., Luu, D.T., Da Ines, O., Casimiro, I., Lucas, M., et al. (2012). Auxin regulates aquaporin function to facilitate lateral root emergence. Nat. Cell Biol. *14*, 991–998. https://doi.org/10.1038/ncb2573.
9. Robbins, N.E., and Dinneny, J.R. (2018). Growth is required for perception of water availability to pattern root branches in plants. Proc. Natl. Acad. Sci. USA *115*, E822–E831. https://doi.org/10.1073/pnas.1710709115.
10. Orosa-Puente, B., Leftley, N., von Wangenheim, D., Banda, J., Srivastava, A.K., Hill, K., Truskina, J., Bhosale, R., Morris, E., Srivastava, M., et al. (2018). Root branching toward water involves posttranslational modification of transcription factor ARF7. Science *362*, 1407–1410. https://doi.org/10.1126/science.aau3956.
11. Mehra, P., Pandey, B.K., Melebari, D., Banda, J., Leftley, N., Couvreur, V., Rowe, J., Anfang, M., De Gernier, H., Morris, E., et al. (2022). Hydraulic flux-responsive hormone redistribution determines root branching. Science *378*, 762–768. https://doi.org/10.1126/science.add3771.
12. Bao, Y., Aggarwal, P., Robbins, N.E., Sturrock, C.J., Thompson, M.C., Tan, H.Q., Tham, C., Duan, L., Rodriguez, P.L., Vernoux, T., et al. (2014). Plant roots use a patterning mechanism to position lateral root branches toward available water. Proc. Natl. Acad. Sci. USA *111*, 9319–9324. https://doi.org/10.1073/pnas.1400966111.
13. Jansen, L., Roberts, I., De Rycke, R., and Beeckman, T. (2012). Phloem-associated auxin response maxima determine radial positioning of lateral roots in maize. Philos. Trans. R. Soc. Lond. B Biol. Sci. *367*, 1525–1533. https://doi.org/10.1098/rstb.2011.0239.
14. Molz, F.J., and Boyer, J.S. (1978). Growth-induced water potentials in plant cells and tissues. Plant Physiol. *62*, 423–429. https://doi.org/10.1104/pp.62.3.423.
15. Alonso-Serra, J., Cheddadi, I., Kiss, A., Cerutti, G., Lang, M., Dieudonné, S., Lionnet, C., Godin, C., and Hamant, O. (2024). Water fluxes pattern

growth and identity in shoot meristems. Nat. Commun. *15*, 6944. https://doi.org/10.1038/s41467-024-51099-x.

16. Bouda, M., Huggett, B.A., Prats, K.A., Wason, J.W., Wilson, J.P., and Brodersen, C.R. (2022). Hydraulic failure as a primary driver of xylem network evolution in early vascular plants. Science *378*, 642–646. https://doi.org/10.1126/science.add2910.
17. Kenrick, P., and Crane, P.R. (1997). The origin and early evolution of plants on land. Nature *389*, 33–39. https://doi.org/10.1038/37918.
18. de Vries, J., and Archibald, J.M. (2018). Plant evolution: landmarks on the path to terrestrial life. New Phytol. *217*, 1428–1434. https://doi.org/10.1111/nph.14975.
19. Kong, L., Liu, Y., Zhi, P., Wang, X., Xu, B., Gong, Z., and Chang, C. (2020). Origins and evolution of cuticle biosynthetic machinery in land plants. Plant Physiol. *184*, 1998–2010. https://doi.org/10.1104/pp.20.00913.
20. Ruszala, E.M., Beerling, D.J., Franks, P.J., Chater, C., Casson, S.A., Gray, J.E., and Hetherington, A.M. (2011). Land plants acquired active stomatal control early in their evolutionary history. Curr. Biol. *21*, 1030–1035. https://doi.org/10.1016/j.cub.2011.04.044.
21. Brodribb, T.J., and McAdam, S.A.M. (2011). Passive origins of stomatal control in vascular plants. Science *331*, 582–585. https://doi.org/10.1126/science.1197985.
22. Chater, C., Kamisugi, Y., Movahedi, M., Fleming, A., Cuming, A.C., Gray, J.E., and Beerling, D.J. (2011). Regulatory mechanism controlling stomatal behavior conserved across 400 million years of land plant evolution. Curr. Biol. *21*, 1025–1029. https://doi.org/10.1016/j.cub.2011.04.032.
23. Pires, N.D., and Dolan, L. (2012). Morphological evolution inland plants: new designs with old genes. Philos. Trans. R. Soc. Lond. B Biol. Sci. *367*, 508–518. https://doi.org/10.1098/rstb.2011.0252.
24. Nieminen, K., Blomster, T., Helariutta, Y., and Mähönen, A.P. (2015). Vascular cambium development. Arabidopsis Book *13*, e0177. https://doi.org/10.1199/tab.0177.
25. De Rybel, B., Mähönen, A.P., Helariutta, Y., and Weijers, D. (2016). Plant vascular development: from early specification to differentiation. Nat. Rev. Mol. Cell Biol. *17*, 30–40. https://doi.org/10.1038/nrm.2015.6.
26. Maurel, C., Verdoucq, L., Luu, D.T., and Santoni, V. (2008). Plant aquaporins: membrane channels with multiple integrated functions. Annu. Rev. Plant Biol. *59*, 595–624. https://doi.org/10.1146/annurev.arplant.59.032607.092734.
27. Chaumont, F., and Tyerman, S.D. (2014). Aquaporins: highly regulated channels controlling plant water relations. Plant Physiol. *164*, 1600–1618. https://doi.org/10.1104/pp.113.233791.
28. Weig, A., Deswarte, C., and Chrispeels, M.J. (1997). The major intrinsic protein family of *Arabidopsis* has 23 members that form three distinct groups with functional aquaporins in each group. Plant Physiol. *114*, 1347–1357. https://doi.org/10.1104/pp.114.4.1347.
29. Chaumont, F., Barrieu, F., Herman, E.M., and Chrispeels, M.J. (1998). Characterization of a maize tonoplast aquaporin expressed in zones of cell division and elongation. Plant Physiol. *117*, 1143–1152. https://doi.org/10.1104/pp.117.4.1143.
30. Maurel, C., Kado, R.T., Guern, J., and Chrispeels, M.J. (1995). Phosphorylation regulates the water channel activity of the seed-specific aquaporin alpha-TIP. EMBO J. *14*, 3028–3035. https://doi.org/10.1002/j.1460-2075.1995.tb07305.x.
31. Johansson, I., Karlsson, M., Shukla, V.K., Chrispeels, M.J., Larsson, C., and Kjellbom, P. (1998). Water transport activity of the plasma membrane aquaporin PM28A is regulated by phosphorylation. Plant Cell *10*, 451–459. https://doi.org/10.1105/tpc.10.3.451.
32. Törnroth-Horsefield, S., Wang, Y., Hedfalk, K., Johanson, U., Karlsson, M., Tajkhorshid, E., Neutze, R., and Kjellbom, P. (2006). Structural mechanism of plant aquaporin gating. Nature *439*, 688–694. https://doi.org/10.1038/nature04316.
33. Meyerowitz, E.M. (1997). Genetic control of cell division patterns in developing plants. Cell *88*, 299–308. https://doi.org/10.1016/s0092-8674(00)81868-1.
34. Greb, T., and Lohmann, J.U. (2016). Plant stem cells. Curr. Biol. *26*, R816–R821. https://doi.org/10.1016/j.cub.2016.07.070.
35. Jill Harrison, C. (2017). Development and genetics in the evolution of land plant body plans. Philos. Trans. R. Soc. Lond. B Biol. Sci. *372*, 20150490. https://doi.org/10.1098/rstb.2015.0490.
36. Harrison, C.J., Roeder, A.H.K., Meyerowitz, E.M., and Langdale, J.A. (2009). Local cues and asymmetric cell divisions underpin body plan transitions in the moss *Physcomitrella patens*. Curr. Biol. *19*, 461–471. https://doi.org/10.1016/j.cub.2009.02.050.
37. Wang, Y., and Li, J. (2008). Molecular basis of plant architecture. Annu. Rev. Plant Biol. *59*, 253–279. https://doi.org/10.1146/annurev.arplant.59.032607.092902.
38. Freudiger, C.W., Min, W., Saar, B.G., Lu, S., Holtom, G.R., He, C., Tsai, J.C., Kang, J.X., and Xie, X.S. (2008). Label-free biomedical imaging with high sensitivity by stimulated Raman scattering microscopy. Science *322*, 1857–1861. https://doi.org/10.1126/science.1165758.
39. Maurel, C., and Chrispeels, M.J. (2001). Aquaporins. A molecular entry into plant water relations. Plant Physiol. *125*, 135–138. https://doi.org/10.1104/pp.125.1.135.
40. Yang, W., Schuster, C., Beahan, C.T., Charoensawan, V., Peaucelle, A., Bacic, A., Doblin, M.S., Wightman, R., and Meyerowitz, E.M. (2016). Regulation of meristem morphogenesis by cell wall synthases in *Arabidopsis*. Curr. Biol. *26*, 1404–1415. https://doi.org/10.1016/j.cub.2016.04.026.
41. Lu, P., Porat, R., Nadeau, J.A., and O'Neill, S.D. (1996). Identification of a meristem L1 layer-specific gene in *Arabidopsis* that is expressed during embryonic pattern formation and defines a new class of homeobox genes. Plant Cell *8*, 2155–2168. https://doi.org/10.1105/tpc.8.12.2155.
42. Sessions, A., Weigel, D., and Yanofsky, M.F. (1999). The *Arabidopsis thaliana* MERISTEM LAYER 1 promoter specifies epidermal expression in meristems and young primordia. Plant J. *20*, 259–263. https://doi.org/10.1046/j.1365-313x.1999.00594.x.
43. Abe, M., Takahashi, T., and Komeda, Y. (2001). Identification of a cis-regulatory element for L1 layer-specific gene expression, which is targeted by an L1-specific homeodomain protein. Plant J. *26*, 487–494. https://doi.org/10.1046/j.1365-313x.2001.01047.x.
44. Takada, S., Takada, N., and Yoshida, A. (2013). ATML1 promotes epidermal cell differentiation in *Arabidopsis* shoots. Development *140*, 1919–1923. https://doi.org/10.1242/dev.094417.
45. Abe, M., Katsumata, H., Komeda, Y., and Takahashi, T. (2003). Regulation of shoot epidermal cell differentiation by a pair of homeodomain proteins in *Arabidopsis*. Development *130*, 635–643. https://doi.org/10.1242/dev.00292.
46. Reynoso, M.A., Kajala, K., Bajic, M., West, D.A., Pauluzzi, G., Yao, A.I., Hatch, K., Zumstein, K., Woodhouse, M., Rodriguez-Medina, J., et al. (2019). Evolutionary flexibility in flooding response circuitry in angiosperms. Science *365*, 1291–1295. https://doi.org/10.1126/science.aax8862.
47. Hancock, A.M., Brachi, B., Faure, N., Horton, M.W., Jarymowycz, L.B., Sperone, F.G., Toomajian, C., Roux, F., and Bergelson, J. (2011). Adaptation to climate across the *Arabidopsis thaliana* genome. Science *334*, 83–86. https://doi.org/10.1126/science.1209244.
48. Exposito-Alonso, M., 500 Genomes Field Experiment Team, Burbano, H.A., Bossdorf, O., Nielsen, R., and Weigel, D. (2019). Natural selection on the Arabidopsis thaliana genome in present and future climates. Nature *573*, 126–129. https://doi.org/10.1038/s41586-019-1520-9.
49. Sutka, M., Li, G., Boudet, J., Boursiac, Y., Doumas, P., and Maurel, C. (2011). Natural variation of root hydraulics in *Arabidopsis* grown in normal and salt-stressed conditions. Plant Physiol. *155*, 1264–1276. https://doi.org/10.1104/pp.110.163113.
50. 1001 Genomes Consortium. Electronic address: magnus.nordborg@gmi.oeaw.ac.at; 1001 Genomes Consortium (2016). 1,135 Genomes Reveal the Global Pattern of Polymorphism in Arabidopsis thaliana. Cell *166*, 481–491. https://doi.org/10.1016/j.cell.2016.05.063.
51. Kang, M., Wu, H., Liu, H., Liu, W., Zhu, M., Han, Y., Liu, W., Chen, C., Song, Y., Tan, L., et al. (2023). The pan-genome and local adaptation of

Arabidopsis thaliana. Nat. Commun. *14*, 6259. https://doi.org/10.1038/s41467-023-42029-4.

52. Chaw, S.M., Chang, C.C., Chen, H.L., and Li, W.H. (2004). Dating the monocot-dicot divergence and the origin of core eudicots using whole chloroplast genomes. J. Mol. Evol. *58*, 424–441. https://doi.org/10.1007/s00239-003-2564-9.
53. Gao, M., He, Y., Yin, X., Zhong, X., Yan, B., Wu, Y., Chen, J., Li, X., Zhai, K., Huang, Y., et al. (2021). Ca^{2+} sensor-mediated ROS scavenging suppresses rice immunity and is exploited by a fungal effector. Cell *184*, 5391–5404.e17. https://doi.org/10.1016/j.cell.2021.09.009.
54. Ito, M., Sentoku, N., Nishimura, A., Hong, S.K., Sato, Y., and Matsuoka, M. (2002). Position dependent expression of GL2-type homeobox gene, Roc1: significance for protoderm differentiation and radial pattern formation in early rice embryogenesis. Plant J. *29*, 497–507. https://doi.org/10.1046/j.1365-313x.2002.01234.x.
55. Wan, Q., Li, Y., Cheng, J., Wang, Y., Ge, J., Liu, T., Ma, L., Li, Y., Liu, J., Zhou, C., et al. (2024). Two aquaporins, PIP1;1 and PIP2;1, mediate the uptake of neonicotinoid pesticides in plants. Plant Commun. *5*, 100830. https://doi.org/10.1016/j.xplc.2024.100830.
56. Bowman, J.L., Kohchi, T., Yamato, K.T., Jenkins, J., Shu, S., Ishizaki, K., Yamaoka, S., Nishihama, R., Nakamura, Y., Berger, F., et al. (2017). Insights into land plant evolution garnered from the *Marchantia polymorpha* genome. Cell *171*, 287–304.e15. https://doi.org/10.1016/j.cell.2017.09.030.
57. Kohchi, T., Yamato, K.T., Ishizaki, K., Yamaoka, S., and Nishihama, R. (2021). Development and molecular genetics of *Marchantia polymorpha*. Annu. Rev. Plant Biol. *72*, 677–702. https://doi.org/10.1146/annurev-arplant-082520-094256.
58. Hirakawa, Y., Fujimoto, T., Ishida, S., Uchida, N., Sawa, S., Kiyosue, T., Ishizaki, K., Nishihama, R., Kohchi, T., and Bowman, J.L. (2020). Induction of multichotomous branching by CLAVATA peptide in *Marchantia polymorpha*. Curr. Biol. *30*, 3833–3840.e4. https://doi.org/10.1016/j.cub.2020.07.016.
59. Sugano, S.S., Nishihama, R., Shirakawa, M., Takagi, J., Matsuda, Y., Ishida, S., Shimada, T., Hara-Nishimura, I., Osakabe, K., and Kohchi, T. (2018). Efficient CRISPR/Cas9-based genome editing and its application to conditional genetic analysis in *Marchantia polymorpha*. PLoS One *13*, e0205117. https://doi.org/10.1371/journal.pone.0205117.
60. Woudenberg, S., Renema, J., Tomescu, A.M.F., De Rybel, B., and Weijers, D. (2022). Deep origin and gradual evolution of transporting tissues: Perspectives from across the land plants. Plant Physiol. *190*, 85–99. https://doi.org/10.1093/plphys/kiac304.
61. McConaha, M. (1941). Ventral structures effecting capillarity in the Marchantiales. Am. J. Bot. *28*, 301–306. https://doi.org/10.1002/j.1537-2197.1941.tb07973.x.
62. Duckett, J.G., Ligrone, R., Renzaglia, K.S., and Pressel, S. (2014). Pegged and smooth rhizoids in complex thalloid liverworts (Marchantiopsida): structure, function and evolution. Bot. J. Linn. Soc. *174*, 68–92. https://doi.org/10.1111/boj.12121.
63. Lu, Y.T., Loue-Manifel, J., Bollier, N., Gadient, P., De Winter, F., Carella, P., Hoguin, A., Grey-Switzman, S., Marnas, H., Simon, F., et al. (2024). Convergent evolution of water-conducting cells in *Marchantia* recruited the *ZHOUPI* gene promoting cell wall reinforcement and programmed cell death. Curr. Biol. *34*, 25. https://doi.org/10.1016/j.cub.2024.01.014.
64. Exposito-Alonso, M., Vasseur, F., Ding, W., Wang, G., Burbano, H.A., and Weigel, D. (2018). Genomic basis and evolutionary potential for extreme drought adaptation in *Arabidopsis thaliana*. Nat. Ecol. Evol. *2*, 352–358. https://doi.org/10.1038/s41559-017-0423-0.
65. Hu, H., and Xiong, L. (2014). Genetic engineering and breeding of drought-resistant crops. Annu. Rev. Plant Biol. *65*, 715–741. https://doi.org/10.1146/annurev-arplant-050213-040000.
66. Heisler, M.G., Ohno, C., Das, P., Sieber, P., Reddy, G.V., Long, J.A., and Meyerowitz, E.M. (2005). Patterns of auxin transport and gene expression during primordium development revealed by live imaging of the *Arabidopsis* inflorescence meristem. Curr. Biol. *15*, 1899–1911. https://doi.org/10.1016/j.cub.2005.09.052.
67. Barbier de Reuille, P., Routier-Kierzkowska, A.L., Kierzkowski, D., Bassel, G.W., Schüpbach, T., Tauriello, G., Bajpai, N., Strauss, S., Weber, A., Kiss, A., et al. (2015). MorphoGraphX: A platform for quantifying morphogenesis in 4D. eLife *4*, 05864. https://doi.org/10.7554/eLife.05864.
68. Larkin, M.A., Blackshields, G., Brown, N.P., Chenna, R., McGettigan, P.A., McWilliam, H., Valentin, F., Wallace, I.M., Wilm, A., Lopez, R., et al. (2007). Clustal W and Clustal X version 2.0. Bioinformatics *23*, 2947–2948. https://doi.org/10.1093/bioinformatics/btm404.
69. Kumar, S., Stecher, G., and Tamura, K. (2016). MEGA7: Molecular Evolutionary Genetics Analysis Version 7.0 for Bigger Datasets. Mol. Biol. Evol. *33*, 1870–1874. https://doi.org/10.1093/molbev/msw054.
70. Han, H., Yan, A., Li, L., Zhu, Y., Feng, B., Liu, X., and Zhou, Y. (2020). A signal cascade originated from epidermis defines apical-basal patterning of *Arabidopsis* shoot apical meristems. Nat. Commun. *11*, 1214. https://doi.org/10.1038/s41467-020-14989-4.
71. Stanislas, T., Platre, M.P., Liu, M., Rambaud-Lavigne, L.E.S., Jaillais, Y., and Hamant, O. (2018). A phosphoinositide map at the shoot apical meristem in *Arabidopsis thaliana*. BMC Biol. *16*, 20. https://doi.org/10.1186/s12915-018-0490-y.
72. Yan, L., Wei, S., Wu, Y., Hu, R., Li, H., Yang, W., and Xie, Q. (2015). High-efficiency genome editing in *Arabidopsis* using *YAO* promoter-driven CRISPR/Cas9 system. Mol. Plant *8*, 1820–1823. https://doi.org/10.1016/j.molp.2015.10.004.
73. Wang, L., Wan, M.C., Liao, R.Y., Xu, J., Xu, Z.G., Xue, H.C., Mai, Y.X., and Wang, J.W. (2023). The maturation and aging trajectory of *Marchantia polymorpha* at single-cell resolution. Dev. Cell *58*, 1429–1444.e6. https://doi.org/10.1016/j.devcel.2023.05.014.
74. Pascut, F.C., Couvreur, V., Dietrich, D., Leftley, N., Reyt, G., Boursiac, Y., Calvo-Polanco, M., Casimiro, I., Maurel, C., Salt, D.E., et al. (2021). Non-invasive hydrodynamic imaging in plant roots at cellular resolution. Nat. Commun. *12*, 4682. https://doi.org/10.1038/s41467-021-24913-z.
75. Ao, J., Fang, X., Miao, X., Ling, J., Kang, H., Park, S., Wu, C., and Ji, M. (2021). Switchable stimulated Raman scattering microscopy with photochromic vibrational probes. Nat. Commun. *12*, 3089. https://doi.org/10.1038/s41467-021-23407-2.
76. Yang, W., Cortijo, S., Korsbo, N., Roszak, P., Schiessl, K., Gurzadyan, A., Wightman, R., Jönsson, H., and Meyerowitz, E. (2021). Molecular mechanism of cytokinin-activated cell division in *Arabidopsis*. Science *371*, 1350–1355. https://doi.org/10.1126/science.abe2305.
77. Zhang, R.B., and Verkman, A.S. (1991). Water and urea permeability properties of Xenopus oocytes: Expression of mRNA from toad urinary bladder. Am. J. Physiol. *260*, C26–C34. https://doi.org/10.1152/ajpcell.1991.260.1.C26.
78. Yu, H., Liu, C., and Dixon, R.A. (2021). A gene-editing/complementation strategy for tissue-specific lignin reduction while preserving biomass yield. Biotechnol. Biofuels *14*, 175. https://doi.org/10.1186/s13068-021-02026-5.
79. Goodstein, D.M., Shu, S., Howson, R., Neupane, R., Hayes, R.D., Fazo, J., Mitros, T., Dirks, W., Hellsten, U., Putnam, N., et al. (2012). Phytozome: a comparative platform for green plant genomics. Nucleic Acids Res. *40*, D1178–D1186. https://doi.org/10.1093/nar/gkr944.
80. Niu, S., Li, J., Bo, W., Yang, W., Zuccolo, A., Giacomello, S., Chen, X., Han, F., Yang, J., Song, Y., et al. (2022). The Chinese pine genome and methylome unveil key features of conifer evolution. Cell *185*, 204–217.e14. https://doi.org/10.1016/j.cell.2021.12.006.
81. Buchfink, B., Reuter, K., and Drost, H.G. (2021). Sensitive protein alignments at tree-of-life scale using DIAMOND. Nat. Methods *18*, 366–368. https://doi.org/10.1038/s41592-021-01101-x.
82. Emms, D.M., and Kelly, S. (2019). OrthoFinder: phylogenetic orthology inference for comparative genomics. Genome Biol. *20*, 238. https://doi.org/10.1186/s13059-019-1832-y.

Please cite this article in press as: Zhu et al., Epidermal hydrodynamics controls water homeostasis of shoot meristems for plant adaptation to terrestrial environments, Developmental Cell (2025), https://doi.org/10.1016/j.devcel.2025.09.007

STAR★METHODS

KEY RESOURCES TABLE

REAGENT or RESOURCE	SOURCE	IDENTIFIER
Antibodies		
Rabbit anti-GFP	Abcam	Cat# ab290; RRID: AB_303395
Goat Anti-Rabbit IgG H&L (HRP)	Abcam	Cat# ab205718; RRID: AB_2819160
Anti-β-Tubulin -HRP	GNI	Cat# GNI4310-BT-S
Bacterial strains		
Escherichia coli DH5a	Weidi Biotechnology	Cat#DL1001
Escherichia coli Rosetta (DE3)	Weidi Biotechnology	Cat#EC1010
Agrobacterium tumefaciens strain GV3101	Weidi Biotechnology	Cat#AC1001
Agrobacterium tumefaciens strain EHA105	Weidi Biotechnology	Cat#AC1010
Saccharomyces cerevisiae strain EGY480	Weidi Biotechnology	Cat#YC1030S
Chemicals, peptides, and recombinant proteins		
TRIzol Reagent	Invitrogen	Cat#15596018
ReverTra Ace qPCR RT Master Mix with gDNA Remover	TOYOBO	Cat#FSQ-301
ChamQ SYBR Color qPCR Master Mix (Without ROX)	Vazyme	Cat#Q421-03
Macerozyme R-10	Yakult Pharmaceutical	CAS: 9032-75-1
Cellulase R-10	Yakult Pharmaceutical	CAS: 9012-54-8
DO Supplement -Leu/-Trp	Clontech	Cat#630417
DO Supplement -His/-Leu/-Trp	Clontech	Cat#630419
DO Supplement -His/-Leu/-Trp/-Ade	Clontech	Cat#630428
Deposited data		
Raw RNA-seq data	This paper	GEO: GSE256367
Exemplar raw SRS data	This paper	Mendeley Data, https://doi.org/10.17632/tnjzrbnsm9.1
OsPIP1;1 gene expression in natural rice accessions	This paper	Mendeley Data, https://doi.org/10.17632/tnjzrbnsm9.1
Fluorescence intensity measurements for ATML1 and PIP2;5 reporters in Arabidopsis	This paper	Mendeley Data, https://doi.org/10.17632/tnjzrbnsm9.1
Experimental models: Organisms/strains		
Arabidopsis: pPIP2;5::GFP-PIP2;5	This paper	N/A
Arabidopsis: pPIP2;5::RFP-PIP2;5	This paper	N/A
Arabidopsis: pATML1:GFP- ATML1	This paper	N/A
Arabidopsis: pPIP1;1::GFP-N7	This paper	N/A
Arabidopsis: pPIP1;2::GFP- N7	This paper	N/A
Arabidopsis: pPIP1;3::GFP- N7	This paper	N/A
Arabidopsis: pPIP1;4::GFP- N7	This paper	N/A
Arabidopsis: pPIP1;5::GFP- N7	This paper	N/A
Arabidopsis: pPIP2;1::GFP-N7	This paper	N/A
Arabidopsis: pPIP2;2::GFP-N7	This paper	N/A
Arabidopsis: pPIP2;3::GFP-N7	This paper	N/A
Arabidopsis: pPIP2;5::GFP-N7	This paper	N/A
Arabidopsis: pPIP2;6::GFP-N7	This paper	N/A
Arabidopsis: pPIP2;7::GFP-N7	This paper	N/A
Arabidopsis: pPIP2;8::GFP-N7	This paper	N/A
Arabidopsis: pTIP1;1::GFP-N7	This paper	N/A

(*Continued on next page*)

Please cite this article in press as: Zhu et al., Epidermal hydrodynamics controls water homeostasis of shoot meristems for plant adaptation to terrestrial environments, Developmental Cell (2025), https://doi.org/10.1016/j.devcel.2025.09.007

Continued

REAGENT or RESOURCE	SOURCE	IDENTIFIER
Arabidopsis: pTIP1;2::GFP-N7	This paper	N/A
Arabidopsis: pTIP2;1::GFP-N7	This paper	N/A
Arabidopsis: pTIP2;2::GFP-N7	This paper	N/A
Arabidopsis: pTIP4;1::GFP-N7	This paper	N/A
Arabidopsis: pPIP2;5-mut::GFP-N7	This paper	N/A
Arabidopsis: pUBQ::GFP-PIP2;5	This paper	N/A
Arabidopsis: pip2;5-CR	This paper	N/A
Arabidopsis: pip2;5 pATML1::GFP-PIP2;5	This paper	N/A
Arabidopsis: pip2;5 pPIP2;5:: GFP-PIP2;5-Hap0	This paper	N/A
Arabidopsis: pip2;5 pPIP2; 5::GFP-PIP2;5-Hap6	This paper	N/A
Arabidopsis: pPIN1::PIN1-GFP	Heisler et al.[66]	N/A
Rice: pOsPIP1;1::GFP-OsPIP1;1	This paper	N/A
Rice: pOsPIP2;1::GFP-OsPIP2;1	This paper	N/A
Rice: pOsPIP2;6::GFP-OsPIP2;6	This paper	N/A
Rice: ospip1;1	Wan et al.[55]	N/A
M. polymorpha: proMpPIP1: MpPIP1-Citrine	This paper	N/A
M. polymorpha: proMpPIP2: MpPIP2-Citrine	This paper	N/A
M. polymorpha: proMpC4HDZ: MpC4HDZ-Citrine	This paper	N/A
M. polymorpha: Mpc4hdz-1	This paper	N/A
M. polymorpha: Mppip1-1 Mppip2-1	This paper	N/A
M. polymorpha Tak-1: Mppip1-2 Mppip2-2	This paper	N/A
Oligonucleotides		
Primers	Table S3	N/A
Recombinant DNA		
1300-pPIP2;5::GFP-PIP2;5	This paper	N/A
1300-pPIP2;5::RFP-PIP2;5	This paper	N/A
1300-pPIP1;1::GFP-N7	This paper	N/A
1300-pPIP1;2::GFP- N7	This paper	N/A
1300-pPIP1;3::GFP- N7	This paper	N/A
1300-pPIP1;4::GFP- N7	This paper	N/A
1300-pPIP1;5::GFP- N7	This paper	N/A
1300-pPIP2;1::GFP-N7	This paper	N/A
1300-pPIP2;2::GFP-N7	This paper	N/A
1300-pPIP2;3::GFP-N7	This paper	N/A
1300-pPIP2;5::GFP-N7	This paper	N/A
1300-pPIP2;6::GFP-N7	This paper	N/A
1300-pPIP2;7::GFP-N7	This paper	N/A
1300-pPIP2;8::GFP-N7	This paper	N/A
1300-pTIP1;1::GFP-N7	This paper	N/A
1300-pTIP1;2::GFP-N7	This paper	N/A
1300-pTIP2;1::GFP-N7	This paper	N/A
1300-pTIP2;2::GFP-N7	This paper	N/A
1300-pTIP4;1::GFP-N7	This paper	N/A
1300-pPIP2;5-mut::GFP-N7	This paper	N/A

(*Continued on next page*)

Please cite this article in press as: Zhu et al., Epidermal hydrodynamics controls water homeostasis of shoot meristems for plant adaptation to terrestrial environments, Developmental Cell (2025), https://doi.org/10.1016/j.devcel.2025.09.007

Continued

REAGENT or RESOURCE	SOURCE	IDENTIFIER
1300-pATML1::GFP- ATML1	This paper	N/A
1300-pATML1::GFP- PIP2;5	This paper	N/A
1300-pPIP2;5::GFP- PIP2;5-Hap0	This paper	N/A
1300-pPIP2;5::GFP- PIP2;5-Hap6	This paper	N/A
pCAMBIA1300-pYAO-PIP2;5-cas9	This paper	N/A
1300-pOsPIP1;1::GFP-OsPIP1;1	This paper	N/A
1300-pOsPIP2;1::GFP-OsPIP2;1	This paper	N/A
1300-pOsPIP2;6::GFP-OsPIP2;6	This paper	N/A
proMpPIP1-MpPIP1-Citrine	This paper	N/A
proMpPIP2-MpPIP2-Citrine	This paper	N/A
proMpC4HDZ::MpC4HDZ-Citrine	This paper	N/A
pTolo-EX1-ATML1-DBD	This paper	N/A
pTolo-EX1-MpC4HDZ-DBD	This paper	N/A
pTolo-EX1-ROC1-DBD	This paper	N/A
pPIP2;5::LUC	This paper	N/A
pOsPIP1;1:LUC	This paper	N/A
pOsPIP1;1-SNP^{C}::LUC	This paper	N/A
pMpPIP1::LUC	This paper	N/A
1300-UBQ10::FLAG-ATML1	This paper	N/A
1300-UBQ10::FLAG-ROC1	This paper	N/A
1300-UBQ10::FLAG-MpC4HDZ	This paper	N/A
pLacZi-pPIP2;5	This paper	N/A
pJG-ATML1	This paper	N/A
1300-pUBQ10::GFP-PIP2;5	This paper	N/A
pOO2-PIP2D	This paper	N/A
pOO2-PIP2Dm	This paper	N/A
pOO2-MpPIP1	This paper	N/A
pOO2-MpPIP2	This paper	N/A
Software and algorithms		
Image J	NIH	https://imagej.net/software/fiji/RRID: SCR_003070
MorphoGraphX	Barbier de Reuille et al.[67]	https://morphographx.org/
GraphPad Prism 8	GraphPad Software, Inc., San Diego, CA, USA	RRID: SCR_002798
Clustal X (1.83)	Larkin et al.[68]	http://www.clustal.org/clustal2/
MEGA7	Kumar et al.[69]	https://megasoftware.net/

EXPERIMENTAL MODEL AND STUDY PARTICIPANT DETAILS

Plant materials and growth conditions

The *Arabidopsis thaliana* ecotype Columbia (Col-0) was used as the wild-type control. The *pip2;5* mutant allele (SAIL_452_H09) was obtained from the collections of the Nottingham Arabidopsis Stock Centre (NASC, United Kingdom). The *atml1-1 pdf2-1* double mutant, Sichuan accession, Tibet accession, and *pUBQ10::29-1-tdTomato* reporter line were described previously.[45,51,70,71] Seeds were surface-sterilized with 70% ethanol/0.05% Triton X-100 for 5 min and 95% ethanol for 1 min. The seeds were then dried under a sterile hood and sown on horizontal plates containing on half-strength Murashige-Skoog medium supplemented with (0.05% MES, 0.8% Phytoagar, pH 5.7 with KOH). After stratification at 4℃ in the dark for 2-3 days, the seed were germinated in a growth chamber under the following conditions: long-day photoperiod (16-h light/8-h dark), light intensity 170 μmoles m^{-2} s^{-1}, day/night temperature 21°C/17 °C. 11-day-old seedlings were transplanted to soil.

For *Marchantia polymorpha* growth, the Tak-1 plants were grown on half-strength solid Gamborg B5 medium supplemented with 1% sucrose under the following conditions: continuous light, 22°C, light intensity 50 ∼ 60 μmol photons m^{-2} s^{-1}.

The rice accession (Zhonghua 11, ZH11) was used as the wild-type control. The *ospip1;1* mutant was described previously.[55] Rice (*Oryza sativa*) plants were grown in protected paddy fields at the Shanghai or Hainan Island experimental stations.

Tobacco (*Nicotiana benthamiana*) plants were grown at 22°C under long-day conditions (16-h day/8-h night) and the leaves of 3∼4-week-old plants were used for transient expression experiments.

Bacterial strains

The *Saccharomyces cerevisiae* strain EGY480 was grown on the YPDA. The *E. coli* strains DH5α and BL21 (DE3) were cultured in LB medium for cloning and protein expression. The *Agrobacterium tumefaciens* EHA105 and GV3101 were cultured in LB medium for plant transformation.

METHOD DETAILS

Plasmid construction

The MultiSite Gateway Three-Fragment Vector Construction system (Invitrogen) was used to generate the translational reporter of *PIP2;5*. A 1,850 bp of the promoter sequence upstream of *PIP2;5* start codon was amplified from Col-0 genomic DNA using the primer pairs PIP2;5_P_GW-F/-R. The PCR product was inserted into pDONR P4-P1R by BP reaction, resulting in 1R4-PIP2;5. A 2,658 bp of the genomic fragment containing the whole coding sequence of *PIP2;5* as well as 1,000 bp 3′ region was amplified with primer pairs PIP2;5_DNA_GW-F/-R. The PCR product was inserted into pDONR P2R-P3, resulting in 2R3-PIP2;5. The coding regions of *GFP* and *RFP* were amplified with primer pairs GFP_GW-F/-R and RFP_GW-F/-R, respectively. The products were inserted into pDONR 221 by BP reaction, resulting in 221-GFP and 221-RFP. 1R4-PIP2;5, 221-GFP, and 2R3-PIP2;5 were incorporated into the binary vector *pH7m34-GW* by LR reaction, resulting in *pPIP2;5::GFP-PIP2;5*. 1R4-PIP2;5, 221-RFP, and 2R3-PIP2;5 were incorporated into the binary vector *pH7m34-GW* by LR reaction, resulting in *pPIP2;5::RFP-PIP2;5*.

For transcriptional reporters, the promoters of aquaporin genes were used to drive the expression of a nuclear localized GFP, GFP-N7. A fragment encoding *GFP-N7* was amplified using the primer pairs GFP_N7-F/-R. The Nos terminator sequence was cloned into *pCAMBIA1300* using primers Nos_1300-F/-R, resulting in *1300-Nos*. The PCR product was inserted into *1300-Nos* by homologous recombination, resulting in *1300-GFP-N7*. The promoters of the aquaporin genes were amplified using the primers listed in Table S3 and ligated into *1300-GFP-N7*, giving rise to *1300-pAQP::GFP-N7*.

For *PIP2;5* promoter mutation, the promoter of *PIP2;5* was amplified using primer pairs pPIP2;5-F/pPIP2;5-mut-R and pPIP2;5-mut-F/pPIP2;5R. The PCR products were ligated into *1300-GFP-N7*, giving rise to *1300-pPIP2;5-mut::GFP-N7*.

For *ATML1* translational reporter, a 3,414 bp of the promoter upstream of *ATML1* start codon was amplified with primer pairs ATML1_P-F/-R. A 717 bp of *GFP* coding region was amplified with primer pairs GFP_ATML1-F/-R. A 3,279 bp genomic fragment containing the coding sequence of *ATML1* as well as 1,000 bp 3′ region was amplified with primer pairs ATML1_DNA-F/-R. The three fragments were ligated into *pCAMBIA1300* by homologous recombination, giving rise to *1300-pATML1::GFP- ATML1*.

For *pATML1::GFP-PIP2;5*, a 3,414 bp of the promoter upstream of *ATML1* start codon was amplified with primer pairs ATML1_P-F/-R. A 717 bp of *GFP* coding region was amplified with primer pairs GFP_ATML1-F/GFP_PIP2;5-R. A 2,631 bp of the genomic fragment containing the whole coding sequence of *PIP2;5* as well as 1,009 bp 3′ region was amplified with primer pairs GFP_PIP2;5-F/PIP2;5-R. The PCR products were ligated into *pCAMBIA1300* by homologous recombination, giving rise to *1300-pATML1::GFP-PIP2;5*.

For *pPIP2;5::GFP-PIP2;5-Hap0* and *pPIP2;5::GFP-PIP2;5-Hap6*, a 1,850 bp of the promoter sequence upstream of *PIP2;5* start codon was amplified with the primer pairs pPIP2;5-F/pPIP2;5-GFP-R. The *GFP* and *PIP2;5-Hap0* were amplified using the primer pairs pPIP2;5-GFP-F/ GFP_PIP2;5-R and GFP_PIP2;5-F/PIP2;5-R. *PIP2;5-Hap6* was amplified with primer pairs GFP_PIP2;5-F/ PIP2;5-Hap6-R and PIP2;5-Hap6-F/PIP2;5-R. The PCR products were ligated into *pCAMBIA1300* by homologous recombination, giving rise to *1300-pPIP2;5::GFP-PIP2;5-Hap0* and *1300-pPIP2;5::GFP-PIP2;5-Hap6*.

For CRISPR/Cas9 mutation of *PIP2;5*, A 20-bp gene-specific guide RNA sequence targeting the 1st exon of *PIP2;5* was synthesized, annealed, and ligated into *pAtU6-26 gRNA*, which was subcloned into the vector *pCAMBIA1300-pYAO-cas9*.[72] The sequences of the oligos are: pip2;5-CR-F: 5′-ATTGTATTCGACGCTACTGAGCTT-3’ and pip2;5-CR-R:5’-AAACAAGCTCAGTAG CGTCGAATA-3’.

For *MpPIP1*, *MpPIP2*, and *MpC4HDZ* translational reporters, a 1,653 bp of *MpPIP1* promoter, a 3,400 bp of *MpPIP2* promoter, and a 3,970 bp of *MpC4HDZ* promoter were amplified with primer pairs MpPIP1_P-F/-R, MpPIP2_P-F/-R, and MpC4HDZ_P-F/-R. A 1,920 bp genomic fragment containing the whole coding sequence of *MpPIP1*, a 2,017 bp genomic fragment containing the whole coding sequence of *MpPIP2*, and a 3,627 bp genomic fragment containing the whole coding sequence of *MpC4HDZ* were amplified with primer pairs MpPIP1_DNA-F/-R, MpPIP2_DNA-F/-R, and MpC4HDZ_DNA-F/-R. These fragments were introduced into the binary vector LW629 by homologous recombination,[73] resulting in *pro*Mp*PIP1:*Mp*PIP1-Citrine*, *pro*Mp*PIP2:*Mp*PIP2-Citrine*, and *pro*Mp*C4HDZ:*Mp*C4HDZ-Citrine*.

To construct the translational reporters of rice aquaporin genes, the promoter sequences of *OsPIP1;1* (3,000 bp), *OsPIP2;1* (3,000 bp), and *OsPIP2;6* (1,214 bp) were amplified with primer pairs OsPIP1;1_P-F/-R, OsPIP2;1_P-F/-R, and OsPIP2;6_P-F/-R. The coding sequences of *GFP* were amplified using primer pairs GFP_OsPIP1;1-F/-R, GFP_OsPIP2;1-F/-R, and GFP_OsPIP2;6-F/-R. Genomic fragments containing the whole coding sequence of *OsPIP1;1*, *OsPIP2;1*, and *OsPIP2;6* were amplified with primer pairs OsPIP1;1_DNA-F/-R, OsPIP2;1_DNA-F/-R, and OsPIP2;6_DNA-F/-R. All PCR products were introduced into *pCAMBIA1300* by

homologous recombination, resulting in *1300-pOsPIP1;1::GFP-OsPIP1;1*, *1300-pOsPIP2;1::GFP-OsPIP2;1*, and *1300-pOsPIP2;6::GFP-OsPIP2;6*.

The CRISPR/Cas9 system was used to generate the Mp*pip1-1* Mp*pip2-1*, Mp*pip1-2* Mp*pip2-2*, and Mp*c4hdz* mutants. Cas9 was expressed under the control of the *Ubiquitin C* (*Mp3g22950*) promoter. The expression of the gRNAs targeting Mp*PIP1*, Mp*PIP2*, and Mp*C4HDZ* was driven by the Mp*U6* promoter. The sgRNAs were designed using primers Mp*pip1* Mp*pip2* Cas-I/II/III/IV and Mp*c4hdz*-Cas-I/II/III/IV.

Arabidopsis, rice, and *M. polymorpha* transformation

All constructs for *Arabidopsis* and *M. polymorpha* transformation were transformed into *Agrobacterium tumefaciens* GV3101 by the freeze-thaw method. *Arabidopsis* transformation was conducted by floral dipping. *M. polymorpha* gemmae were grown on the half-strength Gamborg B5 solid medium supplemented with 1% sucrose for 6 days. After co-culture with *Agrobacterium* for two days, the plants were grown on Gamborg B5 solid medium containing hygromycin and Timentin for selection of the transformants.

For rice transformation, the binary constructs were transformed into *Agrobacterium tumefaciens* EHA105 and into TP309 calli. More than 12 independent transgenic lines were produced that showed similar expression patterns for each reporter genes.

Protein expression and purification

The coding regions for the DNA binding domains of ATML1 (aa 30-134), MpC4HDZ (aa 1-185), and ROC1 (aa 59-177) were amplified with primer pairs ATML1_DBD-F/R, MpC4HDZ_DBD-F/R, and ROC1_DBD-F/R, respectively. The PCR products were ligated into the pTolo-EX1 vector by homologous recombination, giving rise to *pTolo-EX1-ATML1-DBD*, *pTolo-EX1-MpC4HDZ-DBD*, and *pTolo-EX1-ROC1-DBD*. The constructs were transformed into *E. coli* (Rosetta, DE3). The bacteria were grown in liquid LB medium at 37 °C until OD600 = 0.5. To induce the expression of the recombinant proteins, 0.5 mM isopropyl β-D-thiogalactoside (IPTG) was added to the growth medium and the bacteria were cultured at 18°C for 20 h. The recombinant proteins were purified with Ni-NTA beads.

Confocal microscopy imaging of *Arabidopsis* shoot meristem

The main inflorescence meristems of *Arabidopsis* were used to examine the expression patterns of the transcriptional and translational reporters of the aquaporin genes. At bolting stage, about one centimeter of the shoot apex was cut from the tip. The flower buds and floral primordia at late developmental stages were carefully removed to expose the SAM region. The dissected SAMs were cultured in a box containing fresh MS medium supplemented with sucrose and vitamins. The cell walls were stained with 0.1% propidium iodide (PI) for 2 minutes before imaging.

For long-term time-lapse imaging to track cell division in *Arabidopsis* SAMs, the plants were gently taken out from the soil shortly after bolting. The leaves were removed as much as possible until the SAMs could be observed under microscopy. The dissected SAMs were transferred to boxes containing room-temperature *Arabidopsis* medium and recovered for 12 h in a growth chamber with 16/8-h light/dark cycle. Confocal z-stacks of the SAMs were acquired with a 40 × NA 1.2 long-distance water dipping objective on a Zeiss LSM880. Laser excitations were 488 nm (PI and GFP) and 555 nm (RFP).

Confocal microscopy imaging of rice inflorescence meristem

For live imaging of rice inflorescence meristem, the shoot apex shortly after floral transition (around 45 days) was dissected. The leaves and leaf sheath were carefully removed to expose the floral primordia for imaging.

Confocal microscopy imaging of *M. polymorpha*

For time-course live imaging in *M. polymorpha*, the gemmae were germinated and grew on the half-strength Gamborg B5 solid medium supplemented with 1% sucrose. A confocal stack was collected for each plant every 24 hours. Laser excitation was 488 nm for Citrine and chlorophyll autofluorescence, and the emission wavelengths were 520–550 nm for Citrine and 630–730 nm for chlorophyll autofluorescence.

Confocal data analysis

3-D rendering of the confocal stacks was carried out in Fiji. Cell size measurement and cell lineage tracking were performed in MorphoGraphX following the instructions of the user manual.[67] A surface mesh was extracted from the confocal stacks of the SAMs. The fluorescence signals of the cell boundaries were projected onto the mesh and segmented. The cell size was quantified and shown as a heatmap. To assess cell division activity, confocal stacks of the same SAM collected at different time points were segmented. The daughter cells were assigned with the parent labels. The dividing cells were tracked by using the 'Heat Map Proliferation' tool.

Cell size analysis of shoot meristems during desiccation

When the dissected shoot apical meristems (SAMs) were exposed to the ambient air, the cells underwent rapid desiccation. The morphologies of the epidermal cells of the SAMs were imaged using the Keyence digital microscope (VHX-7000). For cell size analysis,

Please cite this article in press as: Zhu et al., Epidermal hydrodynamics controls water homeostasis of shoot meristems for plant adaptation to terrestrial environments, Developmental Cell (2025), https://doi.org/10.1016/j.devcel.2025.09.007

the captured images were imported into Fiji software (https://imagej.net/software/fiji/). The boundaries of the cells within the central zone of the SAMs were delineated using the Polygon selection tool. Subsequently, the area of each cell was measured and displayed in μm^2.

Stimulated Raman scatter (SRS) microscopy

Raman microspectroscopy (RMS) has recently been used to detect water transport in *Arabidopsis* root.[74] To enable more efficient visualization of hydraulic dynamics in short time intervals, we employed Stimulated Raman scattering (SRS) microscopy leveraging the distinct vibrational spectra of O-H and O-D bonds. The SRS experiments were conducted using a custom-built system.[75] A commercial femtosecond laser system (Insight DS+, Spectra Physics) generated two synchronized pulse trains at 80 MHz. The fixed fundamental output of 1040 nm served as the Stokes beam (~200 fs), while the tunable optical parametric oscillator output (680 to 1300 nm, ~150 fs) served as the pump beam. The pulse durations of the pump and Stokes beams were chirped and stretched by passing through SF57 glass rods (~ 3.8 ps for the pump pulse and ~1.8 ps for the Stokes). The intensity of the stokes beam was modulated at 20 MHz using an electro-optical modulator (EOM, EO-AM-R-20-C2, Thorlabs). Both laser beams were coupled into an upright laser-scanning microscopy (FV1200, Olympus). The combined beams were focused onto the sample by a 25× water immersion (Olympus, U XLPLN25XWMP2 25×, NA 1.05) or a 60× water immersion objective lens (Olympus, UPLSAPO 60XWIR, NA 1.2). The transmission of the forward-going pump and Stokes beams was collected by a high N.A. oil condenser (oil immersion, NA=1.4, Nikon). The stimulated Raman loss (SRL) signal, transmitted through a bandpass filter (CARS ET890/220, Chroma), was detected by a homemade reverse-biased photodiode (PD) and demodulated with a lock-in amplifier (HF2LI, Zurich Instruments) at 20MHz to feed the analog input of the microscopy to form images. Raman peaks were detected at 776 nm wavelength pump beam for O-H bonds and at 825 nm for O-D bonds, corresponding to vibrational bands centered at 2500 cm^{-1} for O-D and 3270 cm^{-1} for O-H, respectively. SRS images were captured at a rate of 0.575 s per frame. For each SAM used in the water flux analysis, we also recorded the SRS signals of C-H bonds at the pump laser of 800 nm, corresponding to the vibrational band cantered at 2910 cm^{-1}, which predominantly labels biomolecules such as lipids, proteins, and polysaccharides. The temporal resolution is of the SRS microscopy is 0.575 s per frame with 320 × 320 pixels per frame and a pixel dwell time of 2 μs. The spatial resolution of the system is approximately 350 nm, and the laser powers were kept as: pump 30 mW and Stokes 40 mW. Please see also Methods S1 for further details of the SRS assay.

Chromatin immunoprecipitation assay

The chromatin immunoprecipitation (ChIP) assay was conducted as described previously.[76] Around 2 g of *pATML1::GFP-ATML1* seedlings were grinded in liquid nitrogen and cross-linked in 1% formaldehyde. After nuclear extraction and chromosome fragmentation, the DNA-protein complex was isolated using an anti-GFP antibody (Ab290, Abcam) in a buffer containing 20 mM Tris-HCl (pH, 8.0), 150 mM NaCl, 2 mM EDTA, 1% Triton X-100, and 1× protease inhibitor cocktail coupled to Magna ChIP® Protein A+G Magnetic Beads (Millipore, 16–663). After ChIP, the DNA-protein complex was eluted with ChIP Elution Buffer (1% SDS, 0.1M NaHCO3) and reverse cross-linked at 65℃ for 6 hours. After proteinase K and RNase treatment, DNA was purified by phenol/chloroform/isoamyl alcohol extraction. qPCR was performed using primers PIP2;5_ChIP-I-F/R, PIP2;5_ChIP-II-F/R, and PIP2;5_ChIP-III.

Electrophoretic mobility shift assay

The electrophoretic mobility shift assay (EMSA) was used to assess the binding affinity of the transcription factors to the target gene promoters. The promoter sequences of *PIP2;5*, *MpPIP1*, *OsPIP1;1-SNP^T*, and *OsPIP1;1-SNP^C* promoter variant containing the putative binding sites of ATML1, MpC4HDZ, and ROC1, respectively, were amplified with gene specific primers. The PCR products were labelled with Cy5 in a second round of PCR using a pair of universal primers. The purified ATML1, MpC4HDZ, and ROC1 recombinant proteins were incubated with 7.5 nM Cy5-labeled DNA probes in a buffer containing 100 mM Tris-HCl, pH 7.6, 250 mM KCl, 25 mM $MgCl_2$, 10 mM EDTA, and 10 mM DTT. The reaction was performed at room temperature for 30 min. Unlabelled DNAs were used in the competition assay. The protein-DNA mixture was fractionated on a 4.5% native gel for 1 hour (0.5 × TBE, 100 V, 4°C cold room). The Cy5 signals were detected by scanning the gels in Typhoon FLA 9000 (FUJIFILM FLA 9000 plus DAGE).

Transactivation assay

The dual luciferase assay was used to assess the influence of ATML1, ROC1, and MpC4HDZ binding on the promoter activities of *PIP2;5*, *OsPIP1;1*, Mp*PIP1*, and Mp*PIP2*, respectively. A 1,402 bp of *PIP2;5* promoter, 1,200 bp of *OsPIP1;1-SNP^T* or *OsPIP1;1-SNP^C* promoter, and a 1,653 bp of Mp*PIP1* promoter were amplified with primer pairs PIP2;5_LUC-F/-R, OsPIP1;1_LUC-F/-R, OsPIP1;1_LUC-F/OsPIP1;1-SNP^C_LUC-R and OsPIP1;1-SNP^C_LUC-F/OsPIP1;1_LUC-R, and MpPIP1_LUC-F/-R. The PCR products were ligated into the pGreenII 0800-LUC vector by homologous recombination, resulting in *pPIP2;5::LUC*, *pOsPIP1;1::LUC*, *pOsPIP1;1-SNP^C::LUC*, and *p*Mp*PIP1::LUC*.

The *UBQ10* promoter sequence was cloned into 1300-Nos using primer pairs UBQ10_1300-F/-R, resulting in *1300-UBQ10::Nos*. The coding sequence of *FLAG* was ligated into *1300-UBQ10::Nos*, resulting in *1300-UBQ10::FLAG*. The full-length genomic sequences of *ATML1*, *ROC1*, and *MpC4HDZ* coding regions were amplified with primers ATML1_FLAG-F/-R, ROC1_FLAG-F/-R, and MpC4HDZ_FLAG-F/-R. The PCR products were introduced into *1300-UBQ10::FLAG* by homologous recombination, giving rise to *1300-UBQ10::FLAG-ATML1*, *1300-UBQ10::FLAG-ROC1*, and *1300-UBQ10::FLAG-*Mp*C4HDZ*.

Please cite this article in press as: Zhu et al., Epidermal hydrodynamics controls water homeostasis of shoot meristems for plant adaptation to terrestrial environments, Developmental Cell (2025), https://doi.org/10.1016/j.devcel.2025.09.007

The constructs *1300-UBQ10::FLAG*, *1300-UBQ10::FLAG-ATML1*, *1300-UBQ10::FLAG-ROC1*, and *1300-UBQ10::FLAG-*Mp*C4HDZ* were transiently expressed in tobacco leaf cells together with the dual luciferase reporters *pPIP2;5::LUC*, *pOsPIP1;1::LUC*, and *p*Mp*PIP1::LUC* through *Agrobacterium* infiltration. The RNA silencing suppressor P19 was also co-expressed to increase gene expression efficiency. The activities of LUC and REN were measured using the Dual-Luciferase Reporter Assay System (Promega) according to the manufacture's instructions.

mRNA *in situ* hybridization

The *PIP2;5* antisense RNA probes were synthesized by *in vitro* transcription using the DIG RNA Labeling Kit (Roche). mRNA *in situ* hybridization was performed on the shoot apices of *Arabidopsis* at bolting stage. The dissected SAMs were fixed in FAA (3.7% formaldehyde, 5% acetic acid, 50% ethanol) at 4 °C overnight. Subsequently, the SAMs were dehydrated in a graded series of ethanol and embedded in wax using the ASP300 embedding machine (Leica Microsystems, GmbH, Germany). The samples were sectioned into 8-μm slices. After dewaxing, rehydration and dehydration, the sections were hybridized with *PIP2;5* RNA probes at 55 °C overnight. Subsequently, the slides were washed in SSC and incubated with an anti-digoxigenin-AP antibody (Roche) for 2 hours at room temperature. The hybridization signals were detected by NBT/BCIP (Roche) colour reaction. Images were taken in an Olympus BX53F microscopy with a UPlanSApo 20x/0.75 N.A. objective and an Olympus DP72 Microscopy Digital Camera.

RNA fluorescence *in situ* hybridization (RNA FISH)

For RNA FISH, sample preparation and hybridisation were carried out similarly to chromogenic *in situ* hybridization, except that anti-digoxigenin-POD (Roche) antibody was used. Hybridization signals were detected using TSA Plus Cy5 Fluorescence System (Perkin – Elmer) following the manufacturer's instructions. DAPI staining was performed by mounting the slices with 1 mg/ml DAPI shortly before observing the *in situ* hybridization signals. Images were acquired using a Leica STELLARIS 5 confocal microscopy equipped with a HC PL APO CS2 20x/0.75 IMM objective. Laser excitation wavelengths were 405 nm for DAPI and 633 nm for Cy5.

Yeast one-hybrid assay

The yeast one-hybrid (Y1H) assay was performed to assess the binding of ATML1 to the *PIP2;5* promoter. *PIP2;5* promoter sequence was amplified with primers PIP2;5_Y1H-F/-R and cloned into the pLacZi vector. The full-length coding sequence of *ATML1* was amplified using primers ATML1_Y1H-F/-R, and the PCR product was ligated into the pJG vector by homologous recombination. *pLacZi-pPIP2;5* and *pJG-ATML1* were co-transformed into the yeast strain EGY480. The transformed yeast cells were grown on synthetic complete medium without tryptophan and histidine (-Trp -His) supplemented with 20 % Galactose, 10% Raffinose and 20 mg/ml X-Gal. The yeast one-hybrid assay was repeated for three times.

RNA sequencing analysis

The inflorescence meristems of wild-type and *pip2;5* plants under various humidity conditions were dissected for transcriptome analysis. Around 36 inflorescence meristems were pooled as one replicate. The libraries were prepared and sequenced using Illumina. The raw reads were trimmed with Trimmomatic v.0.39 with parameters: ILLUMINACLIP:TruSeq3-PE.fa:2:30:10:8:true SLIDINGWINDOW:4:20 LEADING:20 TRAILING:20 MINLEN:50. The quality of the sequencing data was assessed using FastQC v0.12.1 (www.bioinformatics.babraham.ac.uk/projects/fastqc/). Reads were then aligned to the TAIR10 transcriptome using Hisat2 v2.2.1. Expression levels were extracted for each gene using TPMCalculator v0.0.3 and featureCounts v2.0.6. Heatmaps representing hierarchical clustering of genes based on their expression were produced using the statistical programme R.

Gene ontology (GO) enrichment and Kyoto Encyclopedia of Genes and Genomes (KEGG) pathway analysis were conducted in programme R with package ClusterProfiler. The retrieved CDS sequences from TAIR were searched through DIAMOND BLASTX against non-redundant protein sequences (nr) database. The BLAST results, which contained the top 20 blast hits with E-value of 10^{-3} for each sequence, were loaded into Blast2GO Basic for Gene Ontology (GO) mapping and annotation using Gene Ontology file goslim_plant.obo. The default annotation configuration was fixed with a GO weight of 5 and annotation cutoff of 75. Un-annotated CDS with BLAST hits were then annotated again with cutoff of 45. All un-annotated CDS sequences were then collected to retrieve InterProScan GO functional annotations through InterProScan4 against EBI databases. Sequences were also blasted against Kyoto Encyclopedia of Genes and Genomes (KEGG) GENES to retrieve the KEGG Orthology (KO) annotation through KofamKOALA.

Quantitative real-time reverse-transcription PCR (qRT-PCR)

Genes expression levels were examined by quantitative real-time reverse-transcription PCR (qRT-PCR). Total RNA was extracted from shoot apex or seedlings using the RNAprep Pure Plant Plus Kit (TIANGEN) following the manufacturer's instructions. The cDNA synthesis was performed using the ReverTra Ace® qPCR RT Master Mix with gDNA remover kit (TOYOBO). The expression level of each gene was examined with the primers listed in Table S3 and normalized to that of *AtACTIN2* of *Arabidopsis* and *OsActin* of rice. Each experiment was conducted with three biological replicates, which gave similar results.

Immunoblotting assay

The shoot apices of *pPIP2;5::GFP-PIP2;5* transgenic plants subjected to different humidity treatment were used for the immunoblotting assay. Total proteins were extracted using an extraction buffer composed of 150 mM NaCl, 20 mM Tris-HCl (pH 8.0), 1mM EDTA (pH 8.0), 1 % Triton X-100, 0.5 mM PMSF, and 1 × Protease Inhibitor Cocktail (Roche). GFP-PIP2;5 protein was detected by an anti-GFP antibody (Abcam, ab290).

Osmotic permeation assay in *Xenopus laevis* oocytes

An osmotic permeation assay in *Xenopus laevis* oocytes was conducted to compare the water uptake activities of PIP2;5-Hap0, PIP2;5-Hap6, MpPIP1, and MpPIP2. The coding sequence of *PIP2;5* Hap0 was amplified using primers Hap0-F/-R. The coding sequence of *PIP2;5* Hap6 was amplified by site-directed mutagenesis using primers hap6–1F/-1R and hap6–2F/-2R. The coding sequence of Mp*PIP1* and Mp*PIP2* were amplified using primers MpPIP1-F/-R and MpPIP2-F/-R, respectively. The PCR products were introduced into the expression vector *pOO2*. The cRNAs were synthesized using the mMESSAGE mMACHINE™ SP6 Transcription Kit (Invitrogen). *Xenopus laevis* oocytes were isolated and injected with 50 nl of sterile water (control) or an equal volume of cRNA solution. The injected oocytes were cultured for 48 hours to allow for the expression of Hap0 and Hap6 proteins. Oocyte swelling was recorded immediately after being transferred from 200 mosm to 40 mosm ND96 solution.[29] The section area (S) of oocytes was measured in Fiji.

Water permeability per cell was calculated by $P_f = V0(d(V/V0)/dt)/(S0 \times Vw \times (OsMin - OsMout))$ where the initial oocyte volume, V0, is 9×10^{-4} cm^3; the initial oocyte area, S0, is 0.045 cm^2; and the molar volume of water, Vw, is 18 cm^3/mol.[77]

Analysis of transgene copy number

To determine the copy number of the transgenes, a qPCR assay was conducted to quantify the amount of *GFP* DNA, using the *FLC* gene as an endogenous homozygous single-gene control.[78] Five lines for each of the *PIP2;5* and *PIP2;5-mut* promoters that contain single heterozygous transgene insertions were characterized. The T2 progeny of these lines were used for confocal scanning to compare GFP fluorescence intensities between *pPIP2;5::GFP-PIP2;5* and *pPIP2;5-mut::GFP-N7* shoot meristems.

Protoplast swelling assay

To assess the water transport activity of PIP2;5 in plant cells, we conducted the protoplast swelling assay. Stable transgenic plants in which *PIP2;5* was overexpressed under the control of the *Arabidopsis UBQ10* promoter was generated by introducing *GFP-PIP2;5* sequence into *1300-UBQ10::Nos* using primers UBQ10::GFP-PIP2;5-F and UBQ10::GFP-PIP2;5-R. The resulting *pUBQ10::GFP-PIP2;5* transgenic plants were used for protoplast preparation. Protoplasts were isolated from the leaves of one-month-old wild-type and *pUBQ10::GFP-PIP2;5* transgenic plants. For protoplast isolation, the abaxial epidermis of the leaves were peeled oof and digested at 28 °C for 20 min in the enzymatic solution containing 1.5 % (wt/vol) cellulase R10 (Yakult), 0.4% (wt/vol) macerozyme R10 (Yakult), 20 mM MES (pH 5.7), 0.4 M mannitol, 20 mM KCl, and 1 % BSA. The protoplast cells were then cultured in an isotonic solution (600 mOsm) containing 10 mM KCl, 1 mM CaCl2, 8 mM MES, and 540 mM Mannitol, pH 5.7. A hypotonic solution (500 mOsm, 440 mM Mannitol) was added to the protoplasts, and the swelling of the protoplast cells were immediately recorded by Olympus cellSens Standard software.

Whole-genome re-sequencing

The genomic DNA was extracted from ~ 10 g seedlings of NIL$^{PIP2;5\text{-}Sic}$, which was used for library preparation and next-generation sequencing. The depth of sequencing is 5G. The raw sequencing data of the Tibet and Sichuan accessions was obtained from the Genome Sequence Archive (GSA) database under BioProject PRJCA012695. The raw reads were trimmed using Trimmomatic v.0.39 with the following parameters: ILLUMINACLIP:TruSeq3-PE.fa:2:30:10:8:true SLIDINGWINDOW:4:20 LEADING:20 TRAILING:20 MINLEN:50. The quality of the sequencing data was assessed using FastQC v0.12.1 (www.bioinformatics.babraham.ac.uk/projects/fastqc/).

The sequencing reads of NIL$^{PIP2;5\text{-}Sic}$, Tibet, and Sichuan were mapped to the Col-0 reference genome using the bwa-mem2 algorithm of BWA-0.7.18 (r1243). The resulting BAM files were filtered for non-unique and unmapped reads using SAMtools v1.2.0, and duplicate reads were processed using Picard tools 3.3.0 (https://broadinstitute.github.io/picard/). SNP calling was conducted using the Genome Analysis Toolkit GATK 4.6.0.0 with default parameters. After filtering via plink with parameters '–geno 0.1 –maf 0.03 –mind 0.1', a total of 1,631,872 SNPs were retained.

Characterization of PIP and ATML1 orthologues

To investigate the evolutionary relationship between ATML1and PIPs, we selected 13 plant species that represent the evolutionary history of the green lineage. These species include *Chlamydomonas reinhardtii*, *Physcomitrium patens*, *Marchantia polymorpha*, *Pinus tabuliformis*, *Amborella Trichopoda*, *Oryza sativa*, *Zea mays*, *Triticum aestivum*, *Brachypodium distachyon*, *Solanum Lycopersicum*, *Glycine max*, and *Gossypium hirsutum*. The protein sequences of these species were downloaded from Phytozome v13.[79] The protein sequences of *Marchantia polymorpha* and *Pinus tabuliformis* were described previously.[56,80] All-to-all blastp with peptide

sequences was conducted by DIAMOND v2.1.10 with cut-off e-values of 1e-5.[81] The blastp results were then loaded into OrthoFinder v2.5.5 for gene clustering with parameters parameters '-I 1.2'.[82] The single-copy orthologous genes of PIPs and ATML1 were then extracted from these gene lists for gene expression analysis.

QUANTIFICATION AND STATISTICAL ANALYSIS

Quantification of SAM size, cell size, and plant weight was conducted in GraphPad Prism 8 (GraphPad Software, San Diego, CA). All values are presented with means ± SD or means ± SEM. Significance of difference was examined by Student's *t* test and one-way ANOVA test. Individual data points are displayed as box and whisker plots with the error bars representing maximum and minimum values (center line, median; box limits, 25th and 75th percentiles). Exact values of n are indicated in the figures or the legends. Detailed descriptions of quantifications and statistical analyses can be found in the figures, figure legends, or methods section. No methods were used for sample randomization or sample size estimation and no data were excluded from analyses.